Appendix B - Climate Change Assessment

(NOTE: This page intentionally left blank.)

TABLE OF CONTENTS

LIST OF FIGURES

LIST OF TABLES

ACRONYMS

ARIMA.... Auto Regressive Integrated Moving Average

BAY.... Bayesian Change Point

BCSD.... Bias Correction and Spatial Disaggregation Method

CESL.... Comprehensive Evaluation of Projects with Respect to Sea-Level Change

CHAT.... Climate Hydrology Assessment Tool

CM.... Cramer-von-Mises

CMIP3.... Coupled Model Intercomparison Project, Phase 3

CMIP5.... Coupled Model Intercomparison Project, Phase 5

CPD.... Conditional Probability Distribution

CPM.... Critical Path Method

ECB.... Engineering Construction Bulletin

END.... Energy Divisive

ER.... Engineer Regulations

ETL.... Engineer Technical Letter

GCM.... Global Climate Models

H-GAC.... Houston-Galveston Area Council

HUC.... Hydrologic Unit Code

KS.... Kolmogorov-Smirnov

LM.... Lombard Mood

LP.... LaPage

LULC.... Land Use and Land Cover

LW.... Lombard Wilcoxen abrupt

MD.... Mood

MHHW.... Mean Higher High Water

MHRWA .... Metropolitan Houston Regional Watershed Assessment

MSL .... Mean Sea Level

MW .... Mann-Whitney

NAVD88 .... North American Vertical Datum of 1988

NCEI .... National Centers for Environmental Information

NOAA .... National Oceanic and Atmospheric Administration

PB .... Planning Bulletin

PT .... Pettitt

RSLC .... Relative Sea Level Change

SLC .... Sea Level Change

SLM .... Smooth Lombard Mood

SLW .... Smooth Lombard Wilcoxen

USACE .... United States Army Corps of Engineers

USGS .... United States Geological Survey

VA .... Vulnerability Assessment

VIC .... Variable Infiltration Capacity

WOWA .... Weighted Order Weighted Average

(NOTE: This page intentionally left blank.)

1 INTRODUCTION AND BACKGROUND

Long-term natural or anthropogenic driven climate change alters regional thermal, hydrologic, and ecological patterns. The purpose of this analysis is to qualitatively assess climate change impacts in the Metropolitan Houston area, particularly how hydrologic variables have responded to climate change in the past and may respond in the future. The results of this qualitative assessment can be used to increase the resilience of existing and proposed water resources projects addressing varying scales of effectiveness in the project area. The MHRWA area is primarily within Hydrologic Unit Code (HUC) 1204, the Galveston Bay-San Jacinto subregion. The eight-digit HUCs in the area are shown in Figure 1 and listed in Table 1.

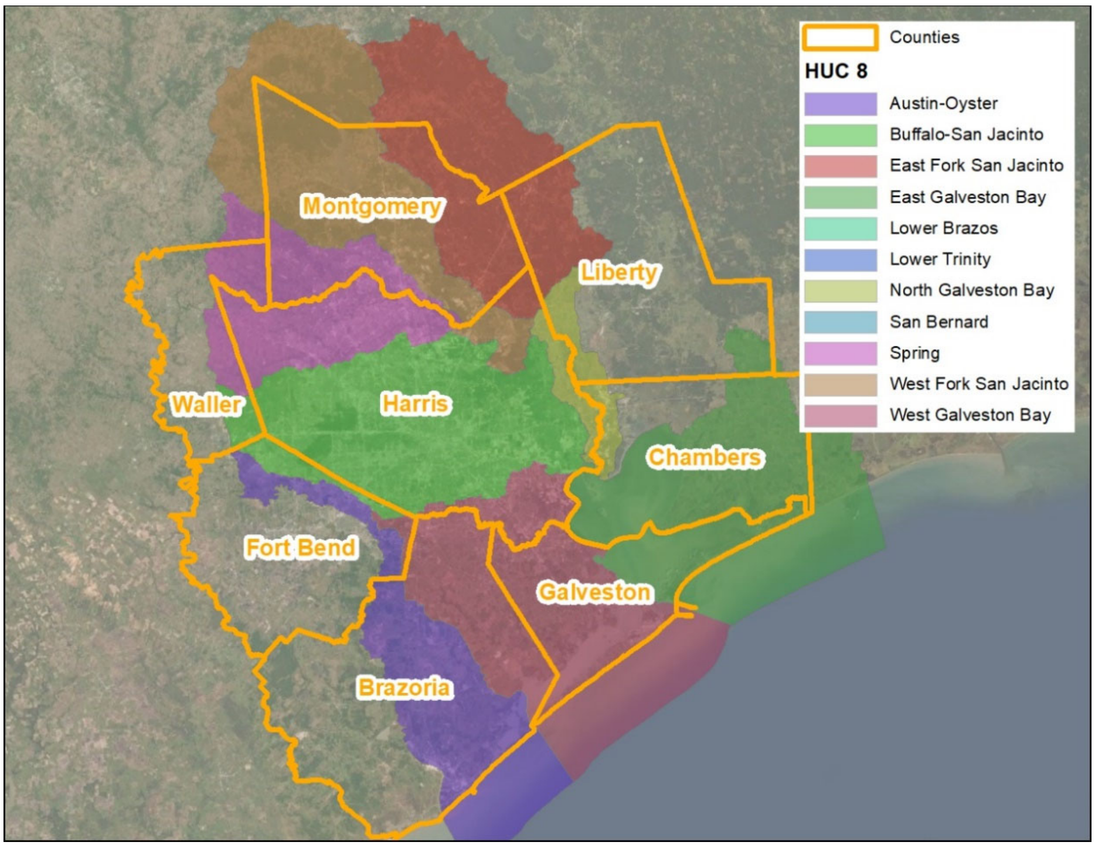

Figure 1: Metro Houston Regional Watershed Assessment Study Area

The outcome of the Metropolitan Houston Regional Watershed Assessment (MHRWA) is a series of recommendations for the area, rather than a specific construction recommendation. As such, and in keeping with the scope of the rest of the project, the climate assessment was done at high level for the region. PB 2019-01 outlines a series of planning steps to be followed when preparing watershed assessments. The climate assessment performed will analyze how climate change variables can potentially impact the resiliency of the study region and potential mitigation efforts that can be implemented to combat climate change impacts. ECB 2018-14 provides guidance for incorporating climate change impacts to inland hydrology particularly related to proposed USACE projects and measures. Although this project does not include an alternatives analysis for construction an implementation, an approach similar to that described in ECB 2018-14 was undertaken to provide a qualitative climate assessment in the area.

Table 1: HUC-8 Focus in the Assessment Area

HUC-8	HUC-8 Description
12040101	Lower Trinity
12040102	West Fork San Jacinto
12040103	Spring
12040104	East Fork San Jacinto
12040202	Buffalo-San Jacinto
12040203	East Galveston Bay
12040204	North Galveston Bay
12040205	West Galveston Bay

2 CLIMATE ASSESSMENT TOOLS

To complete the climate assessment, various tools were utilized for different qualitative analyses. The four different qualitative analyses were Nonstationarity Detection, Climate Hydrologic Assessment Tool, Sea Level Change Curve Calculator, and the Vulnerability Assessment Tool.

2.1 NONSTATIONARITY DETECTION (NSD): TIMESERIES TOOLBOX

The USACE Nonstationarity Detection Timeseries Toolbox (Time Series Toolbox, 2019 http://ec2-34-205-128-255.compute-1.amazonaws.com:8080/tst_app/#shiny-tab-upload_home) was used to determine if statistical tests detected any evidence of nonstationarity in the data. This tool was applied to observed USGS gage data and National Oceanic and Atmospheric Administration (NOAA) climate data. The results from this tool can be found in Section 4.2 and Attachment 1. The Nonstationarity Detection Timeseries Toolbox produces a series of graph and tables to show any potential nonstationarities, changes in statistics, and future trend forecasts. Figure 2 shows an example what each set of graphs look like. Each set of graphs includes a Nonstationarity Detection plot (Graph A), Statistical Method Nonstationarity Test Results plot (Graph B), Statistical Changes plot (Graph C), and ARIMA (forecast of potential trend changes) plot (Graph D). The following sections explain more about how this set of plots are developed.

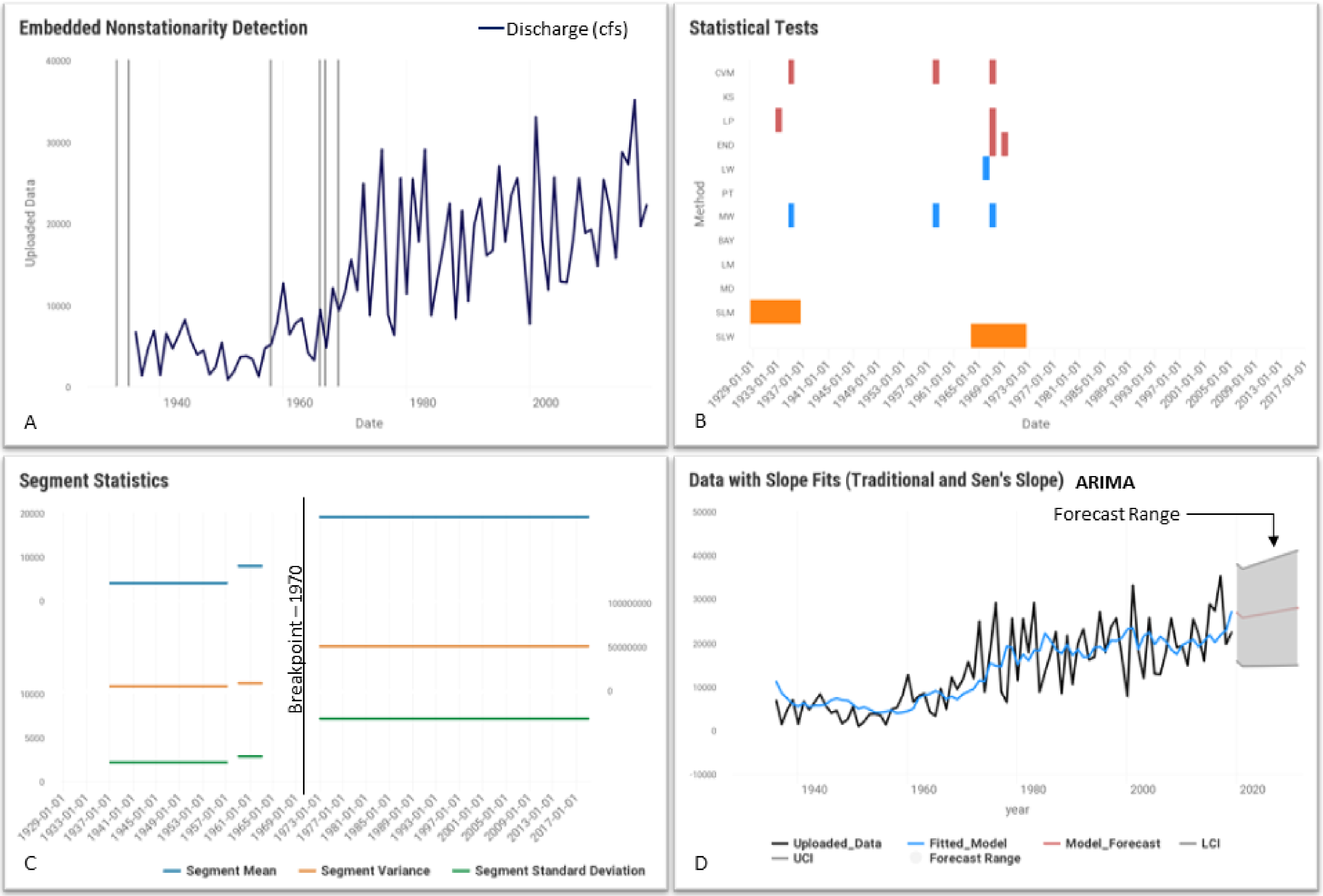

Graph A: Nonstationarity Detection over the analyzed time frame. Graph B: Statistical tests that detected nonstationarity over the analyzed time frame. Graph C: Mean, Variance, Standard Deviation changes over time after nonstationarity detections. Graph D: ARIMA forecast of potential trend in time.

Figure 2: Nonstationarity Plots and ARIMA Plot

2.1.1 Nonstationarity Detection

The Nonstationarity Detection Tool uses a set of default parameters and preprocessing options that can be manipulated as necessary. No parameters or options were manipulated for this climate assessment. This tool produces three graphs. The first graph displays a visualization of the data with the preprocessing applied. Any vertical lines or gaps that appear show times where nonstationarity was detected (fig. 2A). The second graph shows the results from the statistical tests. If any nonstationarities are detected, a red, orange, or blue line will appear to the right of the listed test for the year where the nonstationarity was detected (fig. 2B). The third graph displayed depicts the segment mean, variance, and standard deviation throughout the period of record. As part of the Nonstationarity Detection Tool, a Breakpoint Analysis is conducted to detect breakpoints that may occur in the data by using linear regression models. A line has been added to this plot to show where the Nonstationarity Timeseries Toolbox detected a breakpoint (fig. 2C).

The Time Series Toolbox utilizes a wide range of tests to evaluate the mean, variance, and distribution of the data over time. The Mean-based tests are Lombard Wilcoxen, Pettit, Kolmogorov-Smirnov, and Bayesian Conditional Probability Distribution (CPD). The Variance-based tests are: Mood and Mobard Mood. The Distribution-based tests are Cramer-Von-Mises, Kolmogorov-Smirnov, LePage, and Energy Divisive. The Time Series Toolbox allows for modifying these tests by changing parameters as needed. Increasing the following parameters will decrease sensitivity of the tests resulting in fewer nonstationarities detected: Critical Path Method (CPM), Methods Burn-In Period, CPM Methods Sensitivity, Bayesian Posterior Threshold, and Energy Divisive Method Sensitivity. Decreasing the following parameters will decrease the sensitivity of the tests resulting in few nonstationarities detected: Pettitt Sensitivity, Bayesian Prior Likelihood, and Lombard Smooth Methods Sensitivity. See Figure 2, Graph B for an example of how the plot depicts the statistical tests that detected nonstationarity.

The statistical test name acronyms are: Cramer-von-Mises (CM), Kolmogorov-Smirnov (KS), LaPage (LP), Energy Divisive (END), Lombard Wilcoxen abrupt (LW), Pettitt (PT), Mann-Whitney (MW), Bayesian Change Point (BAY), Lombard Mood (LM), Mood (MD), Smooth Lombard Mood (SLM), and Smooth Lombard Wilcoxen (SLW). The default sensitivity parameters are listed in Table 2.

Table 2 Default Timeseries Toolbox Sensitivity Parameters

Testing Parameter	Value
CPM Methods Burn-In Period	20
CPM Methods Sensitivity	1,000
Bayesian Posterior Threshold	0.5
Energy Divisive Method Sensitivity	0.5
Pettitt Sensitivity	0.05

Testing Parameter	Value
Bayesian Prior Likelihood	0.2
Lombard Smooth Methods Sensitivity	0.05

2.1.2 Trend Analysis

The Time Series Toolbox uses regression techniques on uploaded data. There are two slopes calculated in the Trend Analysis that use two different methods to fit regression curves to the data. The two methods are a traditional slope (least squares regression) and a Sen's slope. For the two slopes, values that are greater than zero correspond to an increasing, positive trend and values less than zero correspond to a negative trend. The trend analysis also uses hypothesis testing to measure the significance of the detected trends in the data. This allows the user to confidently say if there is an existent trend or not. To detect trends, Mann-Kendall and Spearman Rank-Order Tests are utilized.

2.1.3 Time Series Analysis

The Time Series Toolbox uses three types of model choices to complete a time series analysis. They are: Linear Models, Autoregressive Integrated Moving Average (ARIMA), and Exponential Smoothing. For this climate analysis, ARIMA was utilized. ARIMA is the most general class of models for forecasting a time series. It combines both recurring historical patterns (Autoregression) and overall trends (Moving Average) models as well as differencing pre-processing step of the sequence to make the sequence stationary, called integration (I) (USACE, 2019). Figure 2D shows an example of what an ARIMA graph will look like. Each set of analyzed data will have a ARIMA graph that will forecast potential future trends. In most cases, the forecast is a large range indicating that the potential future trends are not that precise and are subject to change based on continued climate change. The three parts of the ARIMA graph that indicate future trends or ranges are LCI, UCI, and Model Forecast. LCI is the Lower Confidence Interval, UCI is the Upper Confidence Interval, and Model Forecast is the mean of LCI and UCI.

2.2 CLIMATE HYDROLOGIC ASSESSMENT TOOL (CHAT)

The USACE CHAT (Climate Hydrology Assessment Tool, 2015, https://corpsmapz.usace.army.mil/apex/f?p=313:2:0::NO:::) was used to show existing conditions and projected changes in relevant climate variables. This tool shows trends in annual maximum peak flow at USGS gages as well as changes in maximum monthly flows. The results from this tool can be found in Section 4.4.

2.2.1 Model Information Supporting CHAT

Modeled projections for temperature, precipitation, and areal runoff were made starting with outputs from the Global Climate Model (GCM) ensembles used in the Coupled Model Intercomparison Project, Phase 5 (CMIP5). These GCM outputs were downscaled using the

Bias Correction and Spatial Disaggregation method (BCSD); monthly BCSD outputs drove the Variable Infiltration Capacity hydrologic model (VIC). Areal hydrologic model outputs are used in the tool, along with the range and trend detection operating on annual maximum monthly flow.

2.2.2 CHAT Steps

This tool has three tabs to view different information. The three tabs are Annual Maximum, Projected Annual Max Monthly, and Mean Projected Annual Max Monthly.

Annual Maximum shows the trend detection in observed annual peak instantaneous streamflow. The information on this tab provides a graphic for the annual peak instantaneous streamflow at a selected United States Geological Survey (USGS) gage within the desired HUC-4 watershed. The graphic provides information on the gage and a link to open the gage data in a separate window. It also includes a trend line that provides the equation for the line and an indication of significance.

Projected Annual Max Monthly shows the climate-modeled projected annual maximum monthly flow range. This tab provides a graphic of the projected climate-changed hydrology for the selected HUC-4 watershed. The range of the 93 projections of annual maximum monthly flow is shown as a yellow range. The mean of the 93 projections of annual maximum monthly flow is shown as a blue line.

The Mean Projected Annual Max Monthly tab shows trend detection in annual maximum monthly flow models. This tab provides a graphic including the statistical analysis of the mean of the projected annual maximum monthly streamflow projections for the selected HUC-4 watershed. It includes a trend line that provides the equation for the line and an indication of significance

2.3 Sea Level Change Curve Calculator

The Seal Level Change (SLC) Curve Calculator (Sea Level Change Curve Calculator, 2014 https://cwbi-app.sec.usace.army.mil/rccslc/slcc_calc.html) was utilized to determine potential SLC scenarios for next century. The SLC Curve Calculator uses the methodology from Engineer Regulation (ER) 1100-2-8162 – Incorporating Sea Level Changes in Civil Works Programs. This calculator consists of a web-based tool that accepts user input such as project start date, selection of appropriate NOAA long term tide gauge, and project life span, to produce a table and graph of the projected sea level changes for the respective project. This tool was developed to calculate the USACE SLC scenarios but can be used to develop other scenarios for comparison purposes. The SLC scenarios in the output are a low, intermediate, and high. For the RSLC assessed in this report, the SLC Curve Calculator tool was used to compute estimated relative sea level change projections at the Galveston Pier 21. The results from the SLC Curve Calculator can be found in Section 4.3.

2.4 VULNERABILITY ASSESSMENT (VA) TOOL

The Vulnerability Assessment Tool (Vulnerability Assessment, 2015 https://maps.crrel.usace.army.mil/apex/f?p=201:1:) was utilized to determine potential future vulnerabilities for the relevant four-digit HUC under dry and wet scenarios and epochs. More information about the specifics of this tool and how it was used can be found in Section 5.1.

The VA Tool produces results of the national screening-level climate assessment for the entire United States at the HUC-4 watershed scale. This is done by using Coupled Model Intercomparison Project 3 (CMIP3) general circulation models. The tool has a set of standard indicators that can be adjusted as needed to show the vulnerabilities based on specific issues a region may face. The assessments can be conducted by business line, at national, regional, and district levels, and for individual indicators. The VA Tool results are seen through maps of vulnerability by planning process and data on how indicators contributed to the vulnerability score by region, epoch, and by timeline for each planning process selected.

3 LITERATURE REVIEW

A literature review of available climate studies and reports was compiled for the study area. Three climate parameters were the focus: temperature, precipitation, and relative sea-level change (RSLC). There was also a limited assessment on land cover changes in the region given the importance on hydrologic variables. USACE published the Recent US Climate Change and Hydrology Literature Applicable to U.S. Army Corps of Engineers Missions – Texas-Gulf Region (two-digit HUC 12) in 2015. This report includes results for exiting conditions and future projections. Figure 3 is pulled from that report and shows the where the consensus lies for different variables including temperature, precipitation, and extreme events.

3.1 TEMPERATURE

Texas has generally seen a historic trend of increasing temperatures (Kunkel et al., 2013; Runkle et al., 2017; Kloesel et al., 2018). Grundstein and Dowd (2011) note an increase in the number of days with extreme maximum and minimum temperatures in addition to average warming trends. The exact estimate for observed temperature increase varies between authors. These include 1 °F since 1900 (Runkle et al., 2017), 1-2 °F since the early 20th century (Kloesel et al., 2018), and a decadal increase of 0.09 °F (Kunkel et al., 2013). Most of the literature reports temperature trends on a state-wide or regional level. Nielsen-Gammon et al. (2020) reports information for Harris County showing a 0.70-0.75 °F per decade increase between 1975-2018 (NCEI nClimDiv Data).

As with historical observation, projected future conditions are generally documented on a state-wide or regional basis. There is consensus that future conditions will likely be warmer than current conditions (Liu et al., 2013; Scherer and Diffenbaugh, 2014; Kunkel et al., 2010; Runkle et al., 2017; Dai et al., 2018; Kloesel et al., 2018; Stoner and Hayhoe, 2020). The extent to which projections are warmer depend on a variety of variables, though most note a significant dependence on the future emissions scenario. Liu et al. (2013) predicts an increase in maximum air temperature of 2 to 5 °C for 2055 compared to the baseline period of 1971-2000 under a scenario with elevated greenhouse gas emissions. Scherer and Diffenbaugh (2014) project steadily increasing temperatures of 5 °C in the summer and 3.2 °C in the winter by 2090. Runkle et al. (2017) includes two projected future temperature ranges based on higher or lower greenhouse gas emissions. The higher emissions scenario projects average temperatures to be 10 °F higher than the historical average and 5 °F higher for the lower emissions scenario. Figure 3 shows the general trends for Texas (two-digit HUC-12) along with the level of scientific consensus on the indicated parameter (USACE, 2015).

3.2 PRECIPITATION

There are two important measures of precipitation, annual precipitation, and precipitation extremes. Average annual precipitation is an important consideration for all water-resources problems; however, precipitation extremes are more significant from a FRM perspective.

Multiple authors have evaluated historical precipitation, with most concluding increasing precipitation over time. The Texas-Gulf Region has experienced a linearly increasing trend in annual precipitation from 1895-2009 (USACE, 2015).

The study area for MHRWA receives approximately 40-60 inches of rain per year. (PRISM Climate Group, 2010). The Houston area has seen a +10-15% increase in precipitation change per century (McRoberts and Nielsen-Gammon, 2011). From 1895-2018, Harris County and surrounding areas saw an increase of 15-21% more precipitation per century (NCEI nClimDiv Data, 2018). Projections for annual and seasonal precipitation are neutral to somewhat mixed compared to projections for other considerations.

The Metro Houston area has been experiencing increases in seasonal precipitation events in the fall and winter (Palecki et al. 2005). According to Texas State Climatologist John Neilson-Gammon, analysis has determined that the frequency of extreme rain events has increased in recent decades (Eye of the Storm, 2018). Neilson-Gammon analyzed US multi-day rainfall records at the 2-, 3-, 5-, and 7-day periods, the average maximum 7-day precipitation and 10 of the greatest storms to occur in the United States. In addition to reviewing rainfall and storm data, Neilson-Gammon refers to a study completed by van Oldenborgh et al (2018) where it was examined that part of the extreme rainfall from Hurricane Harvey can be attributed to climate change through use of the Clausius-Clapeyron relation and the positive trend in intensity of extreme precipitation since 1880. Through all of this, Neilson-Gammon shows that the chances of extreme rainfall have increased (Neilson-Gammon, 2017). This region has been experiencing more frequent intense storms with several record-breaking floods in 2015, 2016, and 2017. In 2017 Hurricane Harvey rewrote the continental U.S. record for total rainfall from a tropical cyclone. A rain gage in the Cedar Bayou watershed (about 30 miles from Houston), recorded 51.88 inches of rain during the multi-day event (NOAA, 2018). Past trends have combined with recent sea surface temperatures, and the heaviest rainfall amounts from intense storms such as Harvey are about 5%-7% greater now than what they were a century ago (NOAA, 2018). Stoner and Hayhoe (2020) also project wetter precipitation extremes.

Figure 3 shows the general trends for Texas (two-digit HUC-12) along with the level of scientific consensus on the indicated parameter (USACE, 2015).

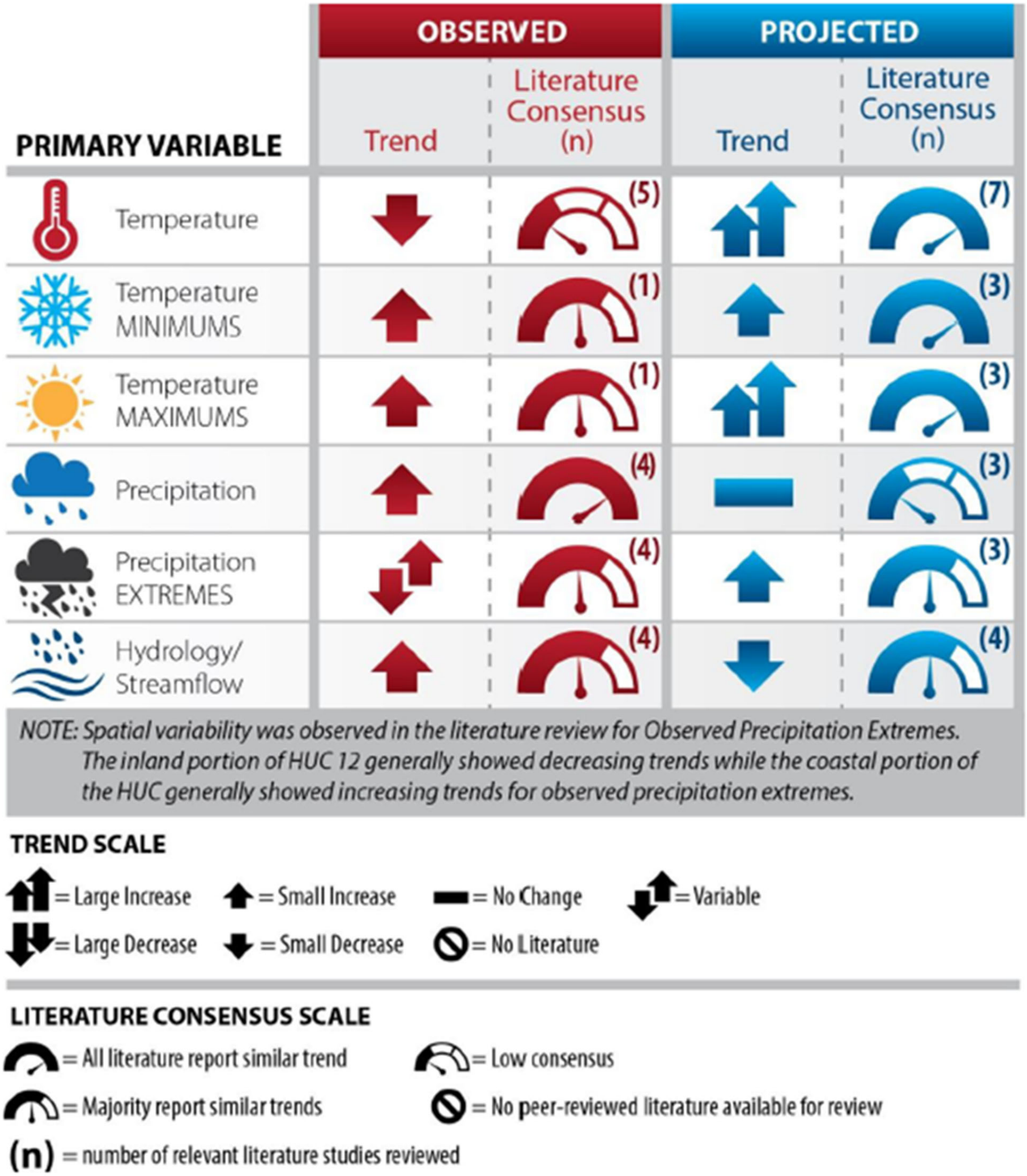

Figure 3: Summary Matrix of Observed and Projected Climate Trends and Literary Consensus

3.3 RELATIVE SEA LEVEL CHANGE

Sea level has been rising along the Texas coast at various rates. The Pier 21 Galveston, TX gage (station ID: 8771450) is the closest to the study area with a long enough historical record to generate relative seal level change (RSLC) trends. The sea-level has been increasing at this location at 0.02096 feet/yr. according to NOAA's 2006 published rates. Figure 4 shows the relative sea level rise mean trend from 1904 to 2020. Figure 5 shows the future projections of RSLC according to USACE 2013 projections for Galveston Pier 21 and Freeport locations. Based on historical trends and available information published from USACE and NOAA regarding future sea level trends, there is consensus that future conditions will continue to see the relative sea level rise along the Texas coast (Paine et al. 2017, NOAA NCEI, 2019).

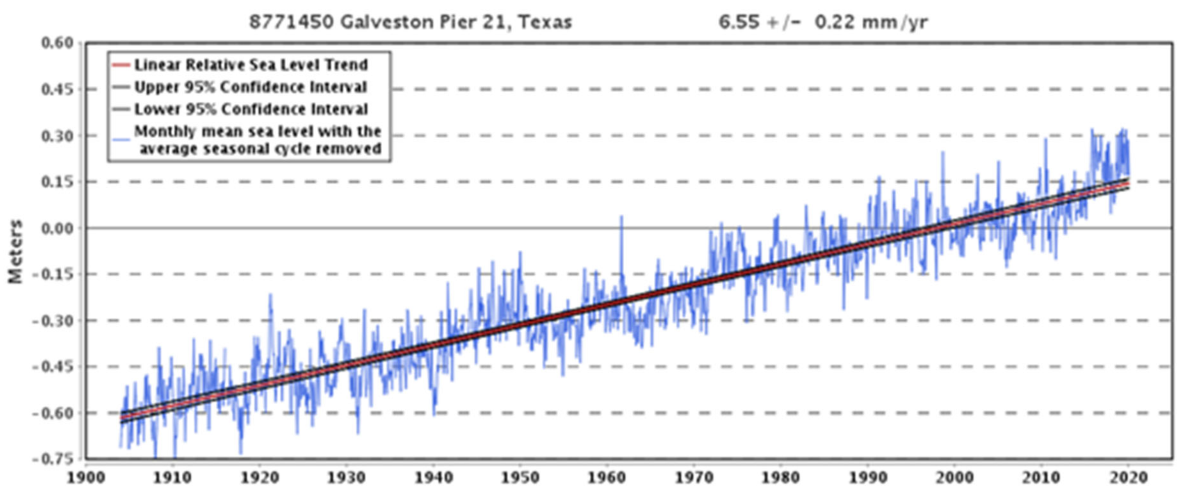

Figure 4: Mean Trends in Sea level Rise at Pier 21, Galveston, TX

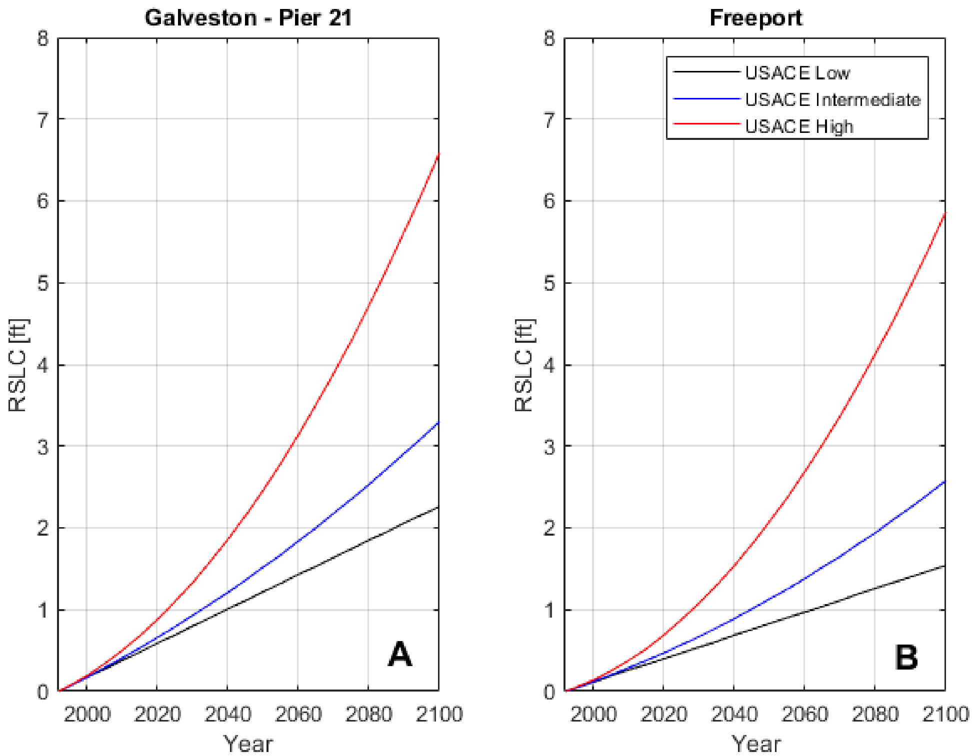

Figure 5: USACE Sea Level Curve Projections for Galveston Pier 21 and Freeport

3.4 LAND USE AND LAND COVER CHANGES

The Houston area has undergone significant urbanization over time throughout the region. Houston's growing population and industries has led to increased impervious areas which can negatively impact the watersheds ability to handle precipitation and promote infiltration. Figure 6 shows the estimated household population growth and the estimated locations of where that population grown will take place (HGAC, 2018). Figure 7 shows a map of parcels with structures built within the Metropolitan Houston Area and then color organized by years built. It is evident that the area has seen a great amount of development since the 1960s.

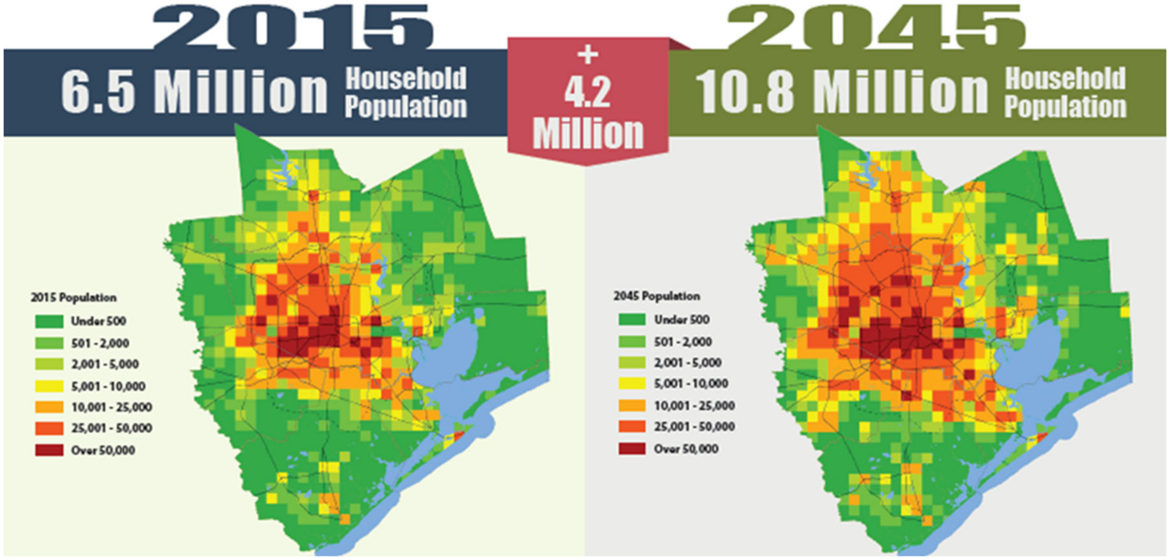

Figure 6: Houston-Galveston Area of Council Projected Population Growth from 2015 to 2045

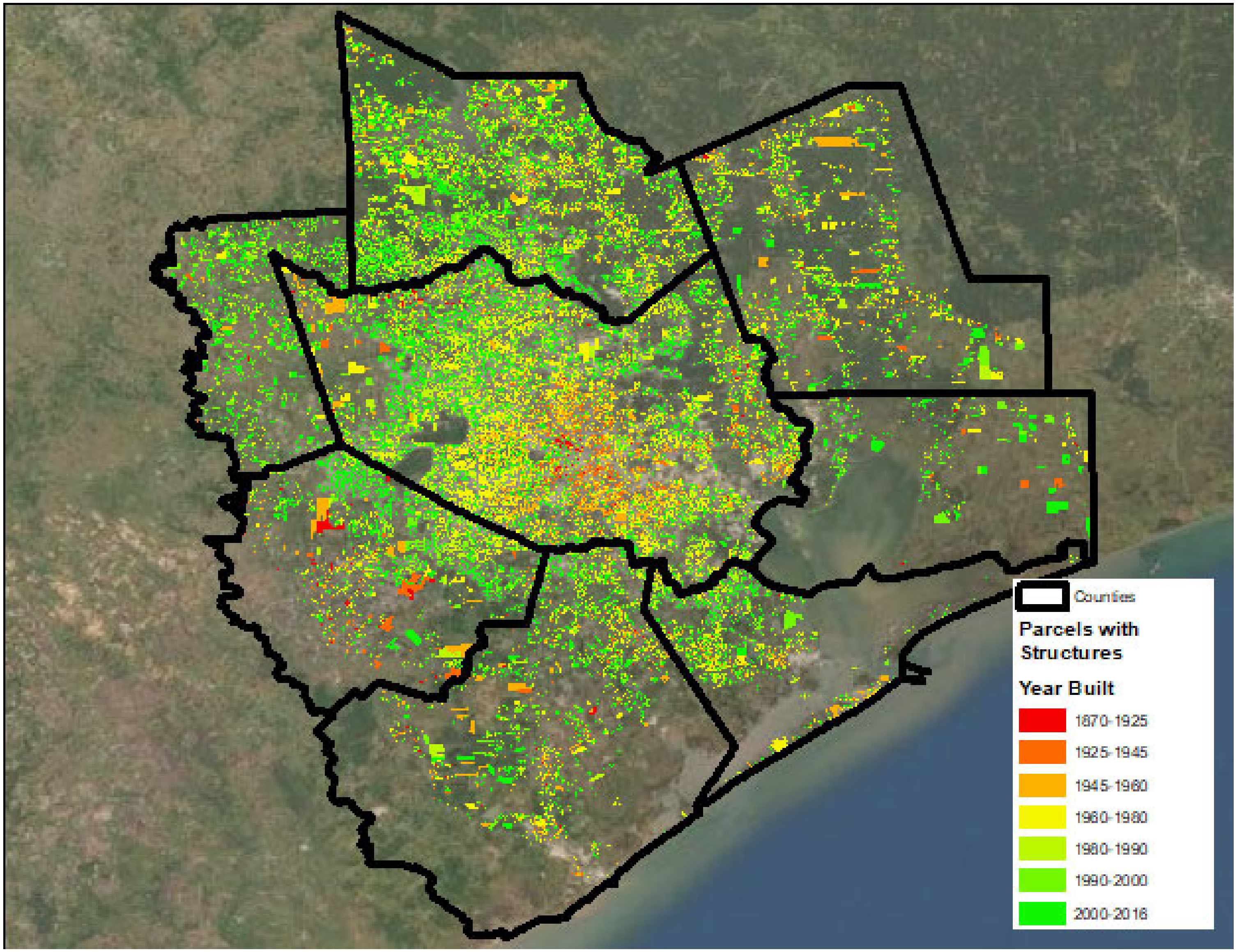

Figure 7: Metropolitan Houston Area – Map of Structures Organized by Year Constructed

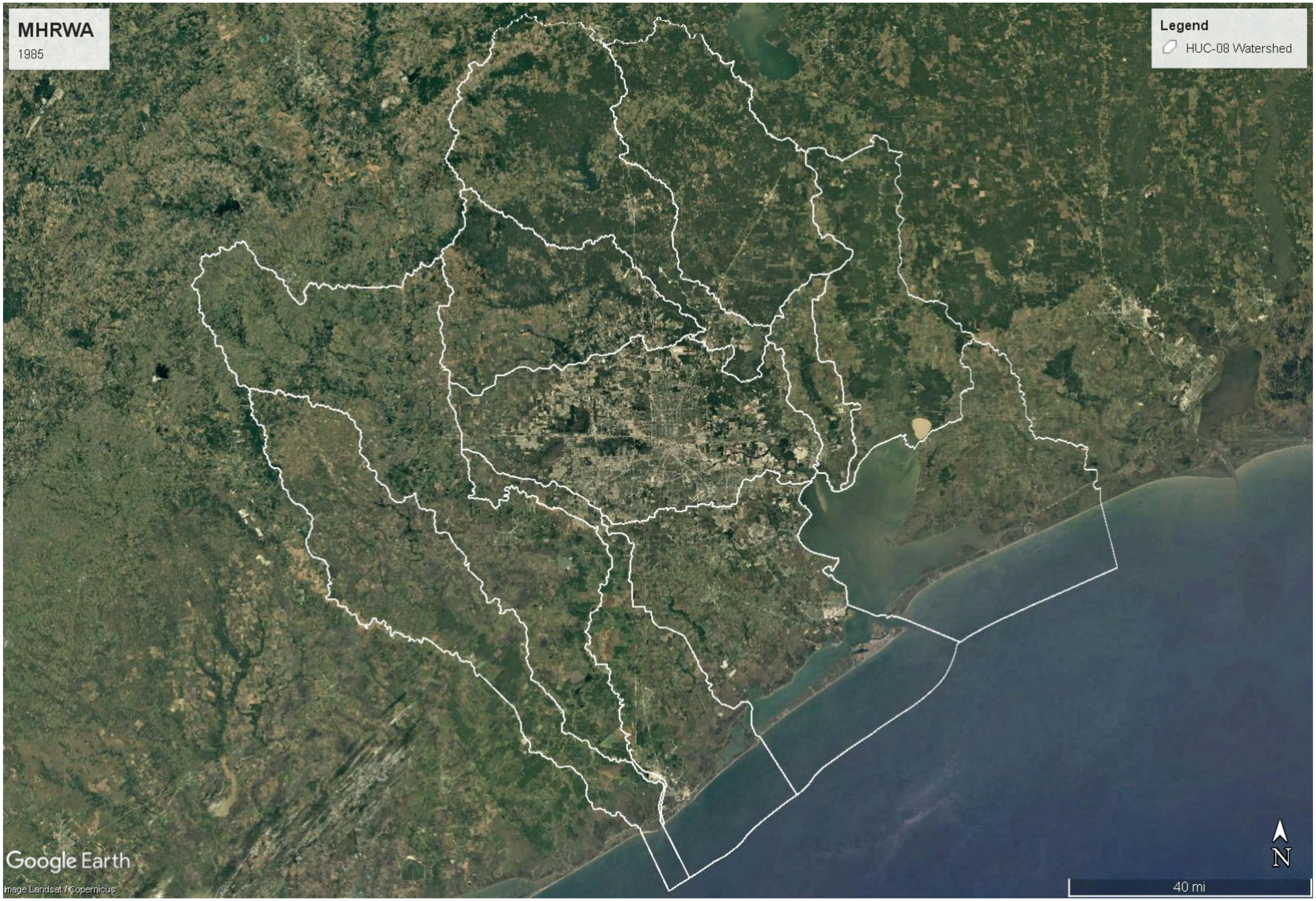

Figure 8 Metropolitan Houston Area – 1985

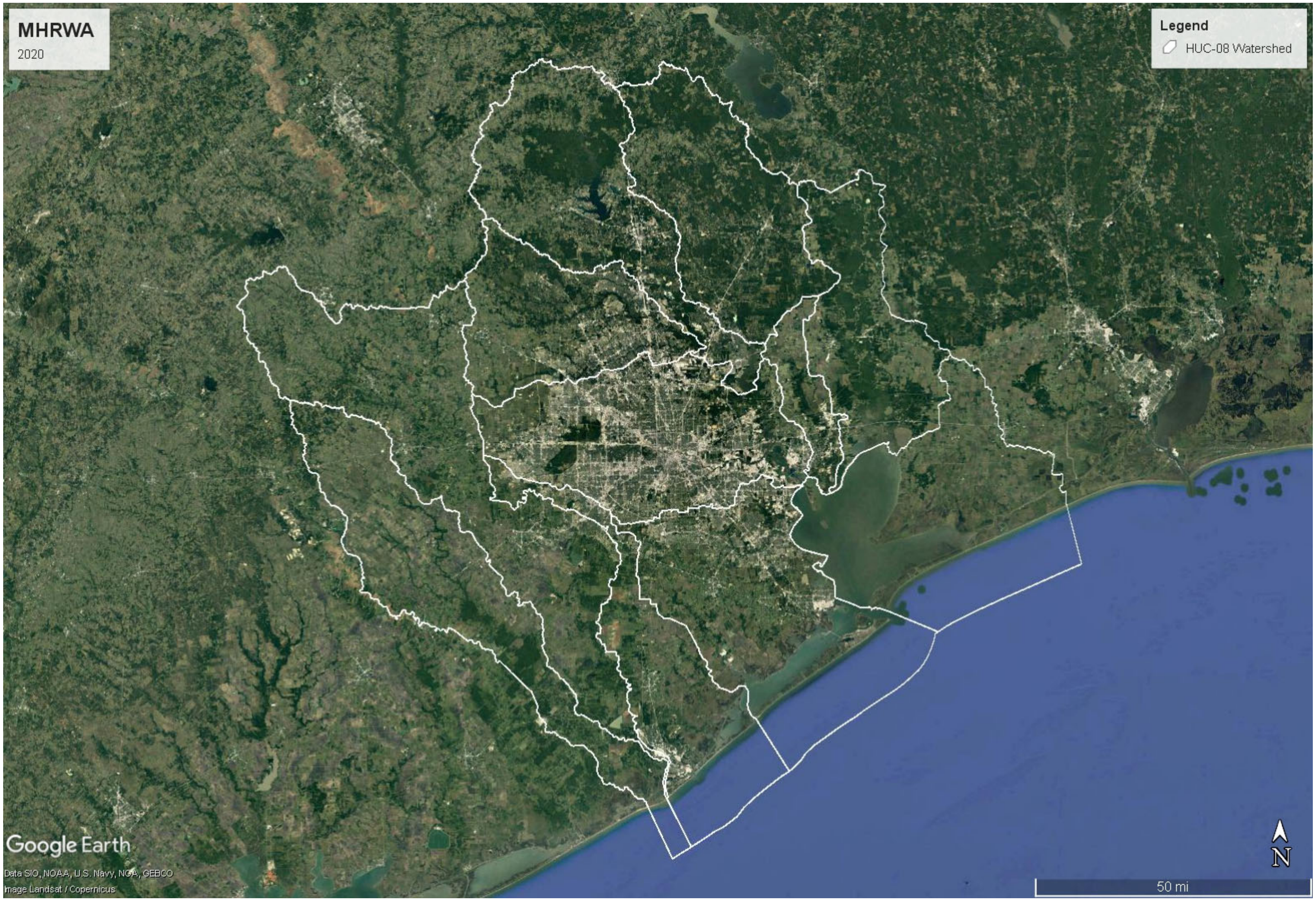

Figure 9 Metropolitan Houston Area – 2020

4 Analysis and Results

4.1 Identification of Relevant Climate Variables

The important hydrological and meteorological variables affecting the project include air temperature, precipitation, stage, and discharge. Not all areas of interest included a long-term gage record. Stream flow magnitudes can be influenced by changes in land-use, channel realignment, and measurement techniques. All factors can potentially make it difficult to determine the role of climate change at the project location. It must be determined if there has been, or will be, a change that affects conditions in the study area and how this change would impact the resilience of project recommendations. Discharge was the major hydrologic variable to analyze for this climate assessment. For areas where appropriate discharge data was unavailable stage was analyzed it its place.

4.2 Site Specific Analysis: Trends in Observed Streamflow Records

This portion of the climate assessment focuses on carrying out first order statistical analyses using stream flow (or stage) observations at USGS gages. The analyzed historical records are listed in Table 3. Figure 10 shows the locations of the gages. There is at least one gage analyzed per watershed, except for HUC 12040202 and HUC 12040203 due to lack of gages with suitable long-term data available.

Table 3: USGS Gage List used in Analyses

USGS Gage List	
08067525	Goose Creek at Baytown, TX
08067000	Trinity River at Liberty, TX
08068000	W Fork San Jacinto River near Conroe, TX
08068090	W Fork San Jacinto River above Lake Houston
08068500	Spring Creek near Spring, TX
08069000	Cypress Ck Nr Westfield, TX
08070500	Caney Ck Nr Splendora, TX
08071280	Luce Bayou Abv Lk Houston Nr Huffman, TX
08074000	Buffalo Bayou at Houston, TX
08074500	Whiteoak Bayou at Houston, TX

USGS Gage List	
08075000	Brays Bayou at Houston, TX
08075730	Vince Bayou at Pasadena, TX
08075770	Hunting Bayou at IH 610, Houston, TX
08077600	Clear Creek near Friendswood, TX
08078000	Chocolate Bayou near Alvin, TX
08115000	Big Creek near Needville, TX
08117500	San Bernard River near Boling, TX

The Nonstationarity Detection Timeseries Toolbox was used to analyze USGS gages located in most of the watersheds involved in this study. In addition to the observed flow records, climate data for annual maximum temperatures and annual precipitation values were analyzed for Harris County. The Harris County data comes from NOAA NCEI Climate at a Glance. Results of the analyses are summarized in Table 4 and full analysis results are available in Attachment 1.

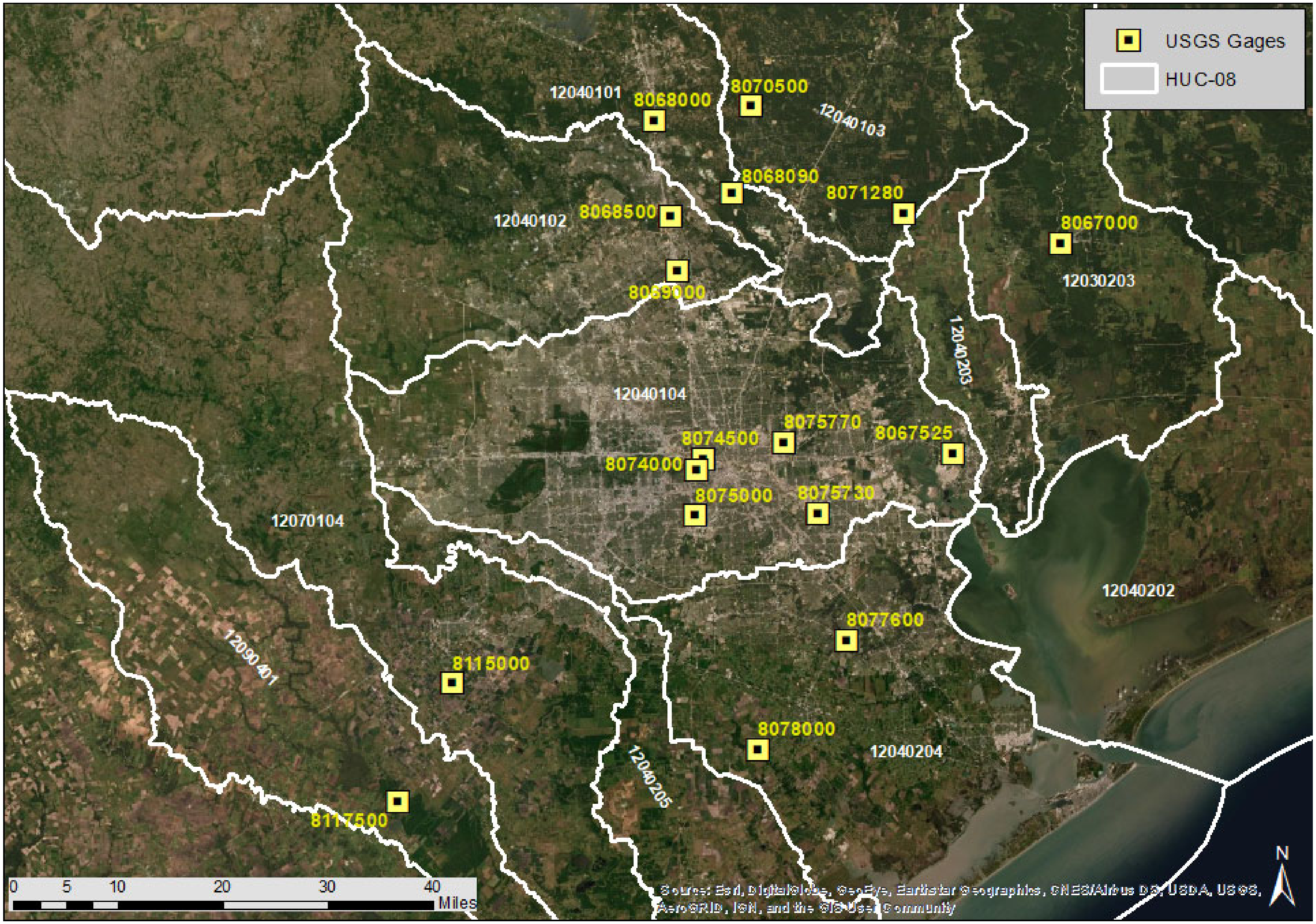

Figure 10: Gage Location Map

Table 4: Summary of breakpoint analysis and statistical significance tests

USGS Gage Number	Gage Location	Breakpoint	Statistical Test p-value			Statistical Significance
			t-test	Mann-Kendall	Spearman R-O	
N/A	Harris Co. Temperature	1997	0.0004	0.0021	0.0018	Significant
N/A	Harris Co. Precipitation	1971	0.004	0.002	0.002	Significant
08067525	Goose Creek at Baytown, TX	1993, 1999	0.29133	0.18376	0.23031	Not Significant
08067000	Trinity River at Liberty, TX	No Breakpoint	0.19626	0.21719	0.18212	Not Significant
08068000	W Fork San Jacinto River near Conroe, TX	No Breakpoint	0.61032	0.68388	0.75455	Not Significant
08068090	W Fork San Jacinto River above Lake					
08068500	Spring Creek near Spring, TX	1990	0.003717	0.0016605	0.001465	Significant
08069000	Cypress Ck Nr Westfield, TX	1990	5.94E-05	8.845E-05	0.000109	Significant
08070500	Caney Ck Nr Splendora, TX	No Breakpoint	0.34899	0.44312	0.46209	Not Significant
08071280	Luce Bayou Abv Lk Houston Nr Huffman, TX					
08074000	Buffalo Bayou at Houston, TX	1941, 2006	0.020402	7.033E-06	2E-05	Significant
08074500	Whiteoak Bayou at Houston, TX	1988	3.45E-11	<2.2e-16	1.00E-15	Significant
08075000	Brays Bayou at Houston, TX	1970	1.97E-16	<2.2e-16	1.72E-18	Significant
08075730	Vince Bayou at Pasadena, TX					
08075770	Hunting Bayou at IH 610, Houston, TX	No Breakpoint	0.004219	0.007702	0.008334	Significant
08077600	Clear Creek near Friendswood, TX					
08078000	Chocolate Bayou near Alvin, TX					
08115000	Big Creek near Needville, TX	2014	0.031837	0.049703	0.042295	Significant
08117500	San Bernard River near Boling, TX					

4.2.1 Harris County – Average Maximum Temperature and Precipitation Analyses

An analysis of Harris County average maximum temperatures and precipitation was completed to look at how the temperature and precipitation has changed in Harris County from 1895 to 2019. The Timeseries Toolbox detected nonstationarities in both average max temperatures and annual precipitation. Figure 11 shows the results of the nonstationarity analysis for the average max temperature and Figures 12 shows the results of the nonstationarity analysis for the annual max precipitation. For the temperature analysis, there is a strong presence of nonstationarities detected from 1993 – 2003. Average max temperatures have continued to increase since then. The nonstationarities for temperature can be attributed to urbanization in the 1990s and early 2000s, potentially increasing hot spots, or heat islands, throughout the region. For precipitation analysis, there was a weak detection of nonstationarities. Since the nonstationarity detection there has been a slightly higher average amount of precipitation each year. The detected nonstationarities can be attributed to rising maximum temperatures and more intense storms bringing larger rainfall. Revised NOAA precipitation statistics show that the frequency of rainfalls is increasing when compared to previous statistics (Perica et al, 2018). The breakpoint analysis determined that the average maximum temperature breakpoint occurred in 1997; the precipitation breakpoint occurred in 1971. ARIMA modeling results predict significantly large range of potentially increasing trends in the future for both Temperature and Precipitation.

Considering the nonstationarities and trend analyses performed, the Time Series Toolbox uses hypothesis testing to measure the significance of the discovered trends in the data. The hypothesis testing allows confirmation of whether a trend exists. P-values for the t-Test, Mann-Kendall, and Spearman Rank-Order tests were computed to determine if there were any significant trends. These results, and those for the other datasets, are compiled Table X. Trends in both datasets for maximum temperature and annual precipitation are statistically significant. This suggests that increasing trends in max temperatures and precipitation are part of chronic climate stressors in this region.

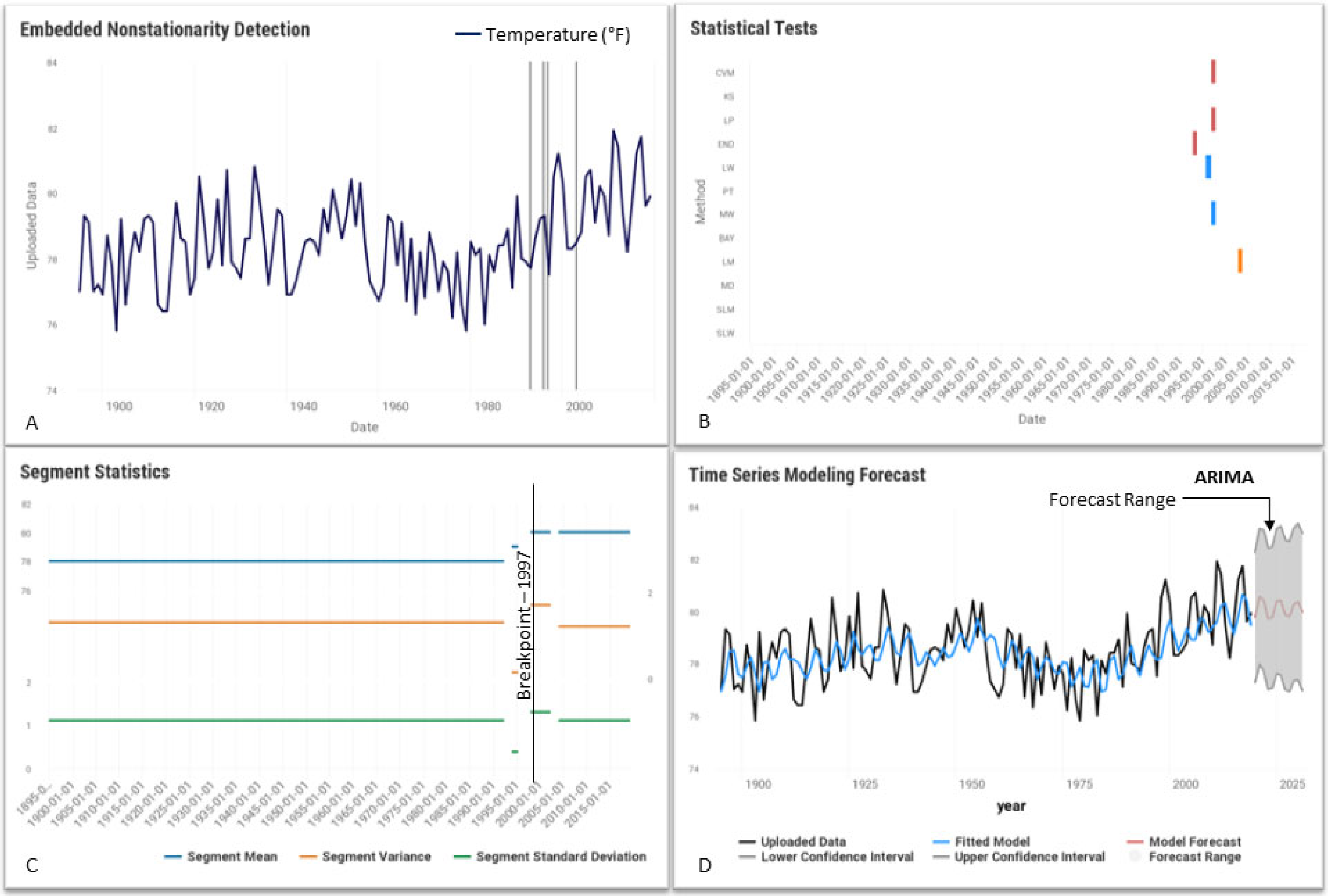

Graph A: Nonstationarity Detection over the analyzed time frame. Graph B: Statistical tests that detected nonstationarity over the analyzed time frame. Graph C: Mean, Variance, Standard Deviation changes over time after nonstationarity detections. Graph D: ARIMA forecast of potential trend in time.

Figure 11: Nonstationarity Detection, Statistical Tests, and Forecast Plots for Harris County Temperature

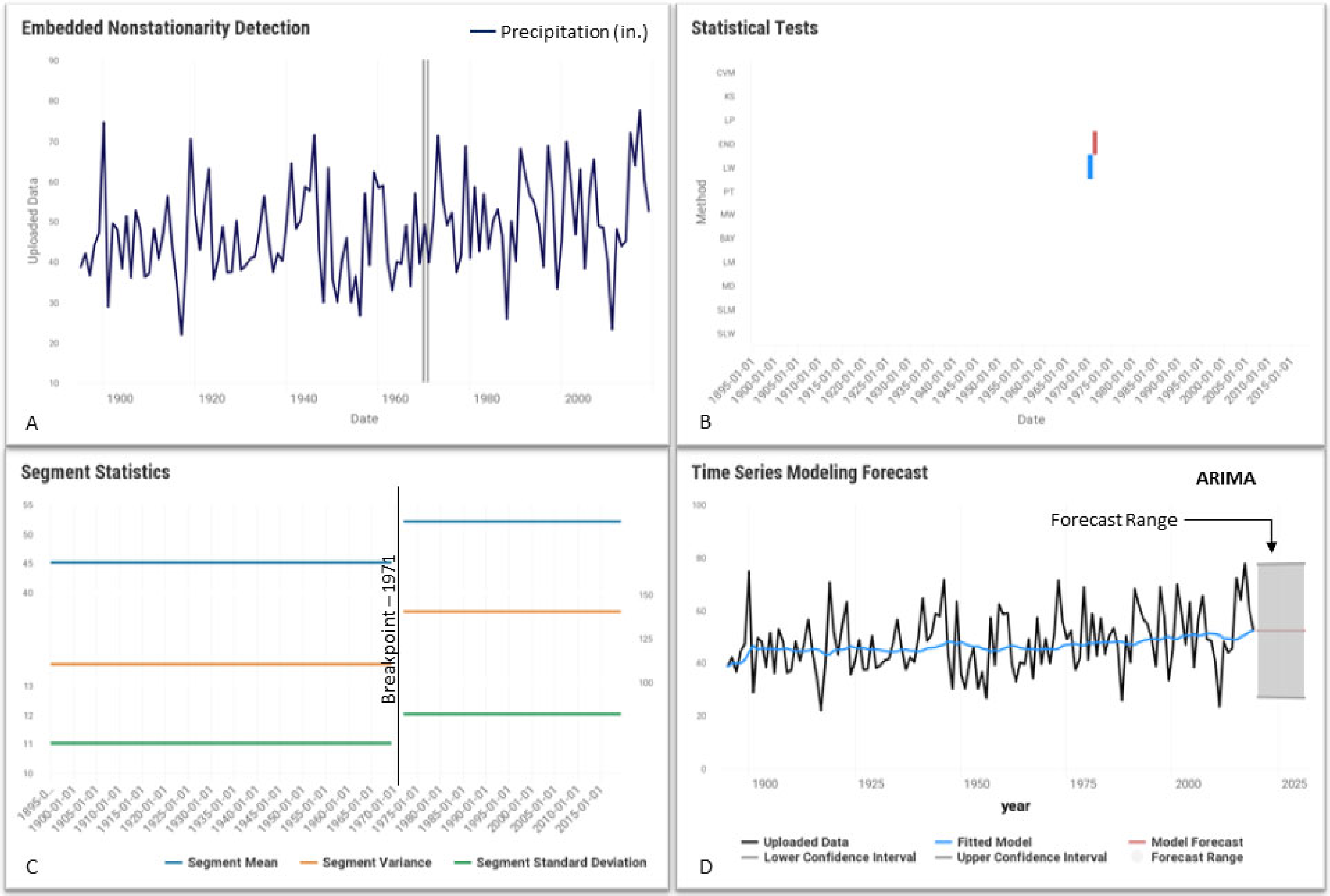

Graph A: Nonstationarity Detection over the analyzed time frame. Graph B: Statistical tests that detected nonstationarity over the analyzed time frame. Graph C: Mean, Variance, Standard Deviation changes over time after nonstationarity detections. Graph D: ARIMA forecast of potential trend in time.

Figure 12: Nonstationarity Detection, Statistical Tests, and Forecast for Harris County Precipitation

4.2.2 Goose Creek at Baytown, TX Analysis (08067525)

An analysis of the furthest downstream gage with suitable data along Goose Creek in HUC 12040104 was completed to look at how the gage height has changed from 1985 to 2021. The USGS gage used for this analysis was 08067525 Goose Creek at Baytown, TX. The Timeseries Toolbox detected several nonstationarities in the gage height for this gage. See Attachment 1 for the results of the statistical tests used to identify potential nonstationarities in the data for Goose Creek. Nonstationarities can be attributed to increased urbanization trends which impact surface and rainfall runoff. The breakpoint analysis determined that the discharge breakpoints occurred in 1993 and 1999. ARIMA model analysis predicts little change in the future stage. Analysis of historic observations are statistically significant for the gage height at this location. See Table 4 for details on summary of breakpoint and statistically significant tests.

4.2.3 Trinity River at Liberty, TX Analysis (08067000)

An analysis of the furthest downstream gage with suitable data along Trinity River in HUC 12030203 was completed to look at how the gage height has changed from 1940 to 2016. The USGS gage used for this analysis was 08067000 Trinity River at Liberty, TX. The Timeseries Toolbox detected nonstationarities in the streamflow for this gage. See Attachment 1 for the results of the statistical tests used to identify potential nonstationarities in the data for Trinity River. Nonstationarities can be attributed to increased urbanization trends which impact surface and rainfall runoff. The lower Trinity River has been and continues to be regulated. Lake Livingston, completed in 1969, is the most proximal to the Houston area. There are also pumping operations on the lower Trinity between Liberty and Wallisville with Coastal Water Authority (CWA) making withdrawals for drinking water supply purposes. The breakpoint analysis determined that there were no breakpoints within this timeframe. ARIMA model analysis predicts little change in the future stage. Analysis of historic observations are not statistically significant for the streamflow at this location. See Table 4 for details on summary of breakpoint and statistically significant tests.

4.2.4 West Fork San Jacinto near Conroe, TX Analysis (08068000)

An analysis of the furthest downstream gage with suitable data along West Fork San Jacinto River in HUC 12040101 was completed to look at how the gage height has changed from 1940 to 2016. The USGS gage used for this analysis was 08068000 West Fork San Jacinto near Conroe, TX. The Timeseries Toolbox detected nonstationarities in the streamflow for this gage. See Attachment 1 for the results of the statistical tests used to identify potential nonstationarities in the data for West Fork San Jacinto. Nonstationarities can be attributed to increased urbanization trends which impact surface and rainfall runoff. The breakpoint analysis determined that there were no breakpoints within this timeframe. ARIMA model analysis predicts little change in the future stage. Analysis of historic observations are not statistically significant for the streamflow at this location. See Table 4 for details on summary of breakpoint and statistically significant tests.

4.2.5 West Fork San Jacinto above Lake Houston, TX Analysis (08068090)

An analysis of the furthest downstream gage with suitable data on West Fork of the San Jacinto River above Lake Houston was completed to look at how the streamflow has changed from 1986 to 2018. The USGS gage used for this analysis was 08068090 West Fork San Jacinto above Lake Houston. The Time Series Toolbox did not detect any nonstationarities at this gage location. At this time, West Fork San Jacinto above Lake Houston represents the current situation and until there is more data collected it will be difficult to detect nonstationarities. See Table 4 for details on summary of breakpoint and statistically significant tests.

4.2.6 Spring Creek near Spring, TX Analysis (08068500)

An analysis of the furthest downstream gage with suitable data along Spring Creek in HUC 12040102 was completed to look at how the streamflow has changed from 1940 to 2016. The USGS gage used for this analysis was 08068500 Spring Creek near Spring, TX. The Timeseries Toolbox detected nonstationarities in the streamflow for this gage. See Attachment 1 for the results of the statistical tests used to identify potential nonstationarities in the data for Spring Creek. Nonstationarities can be attributed to increased urbanization trends which impact surface and rainfall runoff. The breakpoint analysis determined that the discharge breakpoints occurred in 1990. ARIMA model analysis predicts potentially significant change in the future streamflow. Analysis of historic observations are statistically significant for the streamflow at this location. See Table 4 for details on summary of breakpoint and statistically significant tests.

4.2.7 Cypress Creek Near Westfield, TX Analysis (08069000)

An analysis of the furthest downstream gage with suitable data along Cypress Creek in HUC 12040102 was completed to look at how the streamflow has changed from 1945 to 2017. The USGS gage used for this analysis was 08069000 Cypress Creek near Westfield, TX. The Timeseries Toolbox detected significant nonstationarities in the streamflow for this gage. See Attachment 1 for the results of the statistical tests used to identify potential nonstationarities in the data for Cypress Creek. Nonstationarities can be attributed to increased urbanization trends which impact surface and rainfall runoff. The breakpoint analysis determined that the discharge breakpoints occurred in 1990. ARIMA model analysis predicts potentially increasing trends in the future streamflow. Analysis of historic observations are statistically significant for the streamflow at this location. See Table 4 for details on summary of breakpoint and statistically significant tests.

4.2.8 Caney Creek near Splendora, TX Analysis (08070500)

An analysis of the furthest downstream gage with suitable data along Caney Creek in HUC 12040103 was completed to look at how the streamflow has changed from 1945 to 2017. The USGS gage used for this analysis was 08070500 Caney Creek near Splendora, TX. The Timeseries Toolbox detected nonstationarities in the streamflow for this gage. See Attachment 1 for the results of the statistical tests used to identify potential nonstationarities in the data for Caney Creek. Nonstationarities can be attributed to increased urbanization trends which impact surface and rainfall runoff. The breakpoint analysis determined that there were no breakpoints within this timeframe. ARIMA model analysis predicts a similar trend in the future streamflow.

Analysis of historic observations are not statistically significant for the streamflow at this location. See Table 4 for details on summary of breakpoint and statistically significant tests.

4.2.9 Luce Bayou above Lake Houston near Huffman, TX Analysis (08071280)

An analysis of the furthest downstream gage with suitable data on Luce Bayou was completed to look at how the streamflow has changed from 1985 to 2019. The USGS gage used for this analysis was 08071280 Luce Bayou above Lake Houston near Huffman, TX. The Time Series Toolbox did not detect any nonstationarities at this gage location. At this time, Luce Bayou represents the current situation and until there is more data collected it will be difficult to detect nonstationarities. See Table 4 for details on summary of breakpoint and statistically significant tests.

4.2.10 Buffalo Bayou at Houston, TX Analysis (08074000)

An analysis of the furthest downstream gage with suitable data along Buffalo Bayou in HUC 12040104 was completed to look at how the streamflow has changed from 1929 to 2017. The USGS gage used for this analysis was 08074000 Buffalo Bayou at Houston, TX. The Timeseries Toolbox detected significant nonstationarities in the streamflow for this gage. See Attachment 1 for the results of the statistical tests used to identify potential nonstationarities in the data for Buffalo Bayou. Nonstationarities can partially be attributed to increased urbanization trends which impact surface and rainfall runoff. The construction and operation of the Addicks and Barker reservoirs, which regulate flow to Buffalo Bayou, are likely sources of nonstationarity in the record. The breakpoint analysis determined that the discharge breakpoints occurred in 1941 and 2006. The former breakpoint is likely related to construction of the reservoirs which occurred during the 1940s. be attributed to increased urbanization trends which impact surface and rainfall runoff. The breakpoint analysis determined that the discharge breakpoints occurred in 1941 and 2006. ARIMA model analysis predicts potentially increasing trends in the future streamflow. Analysis of historic observations are statistically significant for the streamflow at this location. See Table 4 for details on summary of breakpoint and statistically significant tests.

4.2.11 White Oak Bayou at Houston, TX Analysis (08074500)

An analysis of the furthest downstream gage with suitable data along White Oak Bayou before the confluence at Buffalo Bayou in HUC 12040104 was completed to look at how the streamflow has changed from 1929 to 2017. The USGS gage used for this analysis 08074500 White Oak at Houston, TX. The Timeseries Toolbox detected significant nonstationarities in the streamflow for this gage. See Attachment 1 for the results of the statistical tests used to identify potential nonstationarities in the data for White Oak Bayou. Nonstationarities can be attributed to increased urbanization trends which impact surface and rainfall runoff. There have also been significant conveyance upgrades along the stream during much of the period of record which impacts which is another potential source of nonstationarity. The breakpoint analysis determined that the discharge breakpoints occurred in 1998. This breakpoint is potentially associated with the conveyance improvements, though may not be directly correlated in that 1998 was near the beginning of construction of the federal project. The breakpoint analysis determined that the discharge breakpoints occurred in 1988. ARIMA model analysis predicts potentially increasing trends in the future streamflow. Analysis of historic observations are statistically significant for the streamflow at this location. See Table 4 for details on summary of breakpoint and statistically significant tests.

4.2.12 Brays Bayou at Houston, TX Analysis (08075000)

An analysis of the furthest downstream gage with suitable data along Brays Bayou in HUC 12040104 was completed to look at how the streamflow has changed from 1929 to 2017. The USGS gage used for this analysis 08075000 Brays Bayou at Houston, TX. The Timeseries Toolbox detected significant nonstationarities in the streamflow for this gage. See Attachment 1 for the results of the statistical tests used to identify potential nonstationarities in the data for Brays Bayou. Nonstationarities can be attributed to increased urbanization trends which impact surface and rainfall runoff. There have also been significant conveyance upgrades along the stream during much of the period of record which impacts which is another potential source of nonstationarity. The breakpoint analysis determined that the discharge breakpoints occurred in 1970. This breakpoint is potentially associated with the conveyance improvements constructed during the first round of improvements around that time. The breakpoint analysis determined that the discharge breakpoints occurred in 1970. ARIMA model analysis predicts significant increasing trends in the future streamflow. Analysis of historic observations are statistically significant for the streamflow at this location. See Table 4 for details on summary of breakpoint and statistically significant tests.

4.2.13 Vince Bayou at Pasadena, TX Analysis (08075730)

An analysis of the furthest downstream gage with suitable data on Vince Bayou was completed to look at how the streamflow has changed from 1972 to 2018. The USGS gage used for this analysis was 08075730 Vince Bayou at Pasadena, TX. The Time Series Toolbox did not detect any nonstationarities at this gage location. At this time, Vince Bayou represents the current situation and until there is more data collected it will be difficult to detect nonstationarities. See Table 4 for details on summary of breakpoint and statistically significant tests.

4.2.14 Hunting Bayou at IH-610 Houston, TX Analysis (08075770)

An analysis of the furthest downstream gage with suitable data along Hunting Bayou in HUC 12040104 was completed to look at how the streamflow has changed from 1964 to 2018. The USGS gage used for this analysis 08075770 Hunting Bayou at IH-610 Houston, TX. The Timeseries Toolbox detected nonstationarities in the streamflow for this gage. See Attachment 1 for the results of the statistical tests used to identify potential nonstationarities in the data for Hunting Bayou. Nonstationarities can be attributed to increased urbanization trends which impact surface and rainfall runoff. The breakpoint analysis determined there were no breakpoints within this timeframe. ARIMA model analysis predicts similar trends in the future streamflow. Analysis of historic observations are statistically significant for the streamflow at this location. See Table 4 for details on summary of breakpoint and statistically significant tests.

4.2.15 Clear Creek near Friendswood, TX Analysis (08077600)

An analysis of the furthest downstream gage with suitable data on Clear Creek was completed to look at how the streamflow has changed from 1998 to 2019. The USGS gage used for this analysis was 08077600 Clear Creek near Friendswood, TX. The Time Series Toolbox did not detect any nonstationarities at this gage location. At this time, Clear Creek represents the current situation and until there is more data collected it will be difficult to detect nonstationarities. See Table 4 for details on summary of breakpoint and statistically significant tests.

4.2.16 Chocolate Bayou near Alvin, TX Analysis (08078000)

An analysis of the furthest downstream gage with suitable data on Chocolate Bayou was completed to look at how the streamflow has changed from 1947 to 2019. The USGS gage used for this analysis was 08078000 Chocolate Bayou near Alvin, TX. The Time Series Toolbox did not detect any nonstationarities at this gage location. At this time, Clear Creek represents the current situation and until there is more data collected it will be difficult to detect nonstationarities. See Table 4 for details on summary of breakpoint and statistically significant tests.

4.2.17 Big Creek near Needville, TX Analysis (08115000)

An analysis of the furthest downstream gage with suitable data along Big Creek in HUC 12070104 was completed to look at how the streamflow has changed from 1991 to 2019. The USGS gage used for this analysis 080115000 Big Creek near Needville, TX. The Timeseries Toolbox detected nonstationarities in the streamflow for this gage. See Attachment 1 for the results of the statistical tests used to identify potential nonstationarities in the data for Big Creek. Nonstationarities can be attributed to increased urbanization trends which impact surface and rainfall runoff. The breakpoint analysis determined there that the discharge breakpoints occurred in 2014. ARIMA model analysis predicts potentially increasing trends in the future streamflow. Analysis of historic observations are statistically significant for the streamflow at this location. See Table 4 for details on summary of breakpoint and statistically significant tests.

4.2.18 San Bernard River near Boling, TX Analysis (08117500)

An analysis of the furthest downstream gage with suitable data on San Bernard River was completed to look at how the streamflow has changed from 1955 to 2019. The USGS gage used for this analysis was 08117500 San Bernard River near Boling, TX. The Time Series Toolbox did not detect any nonstationarities at this gage location. At this time, San Bernard represents the current situation and until there is more data collected it will be difficult to detect nonstationarities. See Table 4 for details on summary of breakpoint and statistically significant tests.

4.3 TIDE CHANGE IMPACTS FROM RELATIVE SEA LEVEL CHANGE

There are 10 NOAA water-level and meteorological gauges within the focus area of the study (Figure 13). Daily and extreme tides impact water levels upstream and stage-discharge relationships on bayous and rivers in coastal watersheds within the study area. RLSC will further impact conveyance.

For the focus of this study area, the Galveston Pier 21 NOAA station was used. The tidal datum at Galveston Pier 21, TX (NOAA 8771450), with projections of USACE Sea Level Curves and can be viewed in Table 5. The sea level change rate at Galveston Pier 21 is 0.02096 feet/year from NOAA's 2006 published rates. The projected sea level rise used for the NOAA Sea Level Rise viewer was the 2070 USACE Intermediate Curve of 2.18 ft. and the 2120 USACE Intermediate Curve which is 4.14 ft. Figure 14 shows the migration upstream of the head of tides, projected by USACE Intermediate curves mapping with the NOAA Sea Level Rise viewer for Buffalo and Whiteoak Bayous. To see the results for head of tides for the future projections for Armand Bayou, Brays Bayou, Sims Bayou, Cedar Bayou, Chocolate Bayou, Clear Creek, Dickinson Bayou, Halls Bayou (Brazoria County), Halls Bayou (Harris County), Greens Bayou, Hunting Bayou, San Jacinto River below Lake Houston, and Trinity River, see Attachment 2.

Table 5: USACE Projected Sea Level Curves for Galveston Pier 21 gage (ft, LMSL)

Year	USACE Low	USACE Int.	USACE High
1992	0.00	0.00	0.00
1995	0.06	0.06	0.07
2000	0.17	0.17	0.19
2005	0.27	0.29	0.34
2010	0.38	0.41	0.50
2015	0.48	0.53	0.68
2020	0.59	0.66	0.88
2025	0.69	0.79	1.10
2030	0.80	0.93	1.33
2035	0.90	1.07	1.59
2040	1.01	1.21	1.86
2045	1.11	1.36	2.15
2050	1.22	1.52	2.46
2055	1.32	1.67	2.79

Year	USACE Low	USACE Int.	USACE High
2060	1.43	1.84	3.14
2065	1.53	2.00	3.51
2070	1.64	2.18	3.89
2075	1.74	2.35	4.29
2080	1.85	2.53	4.72
2085	1.95	2.72	5.16
2090	2.06	2.91	5.62
2095	2.16	3.10	6.09
2100	2.26	3.30	6.59
2105	2.37	3.50	7.10
2110	2.47	3.71	7.64
2115	2.58	3.92	8.19
2120	2.68	4.14	8.76

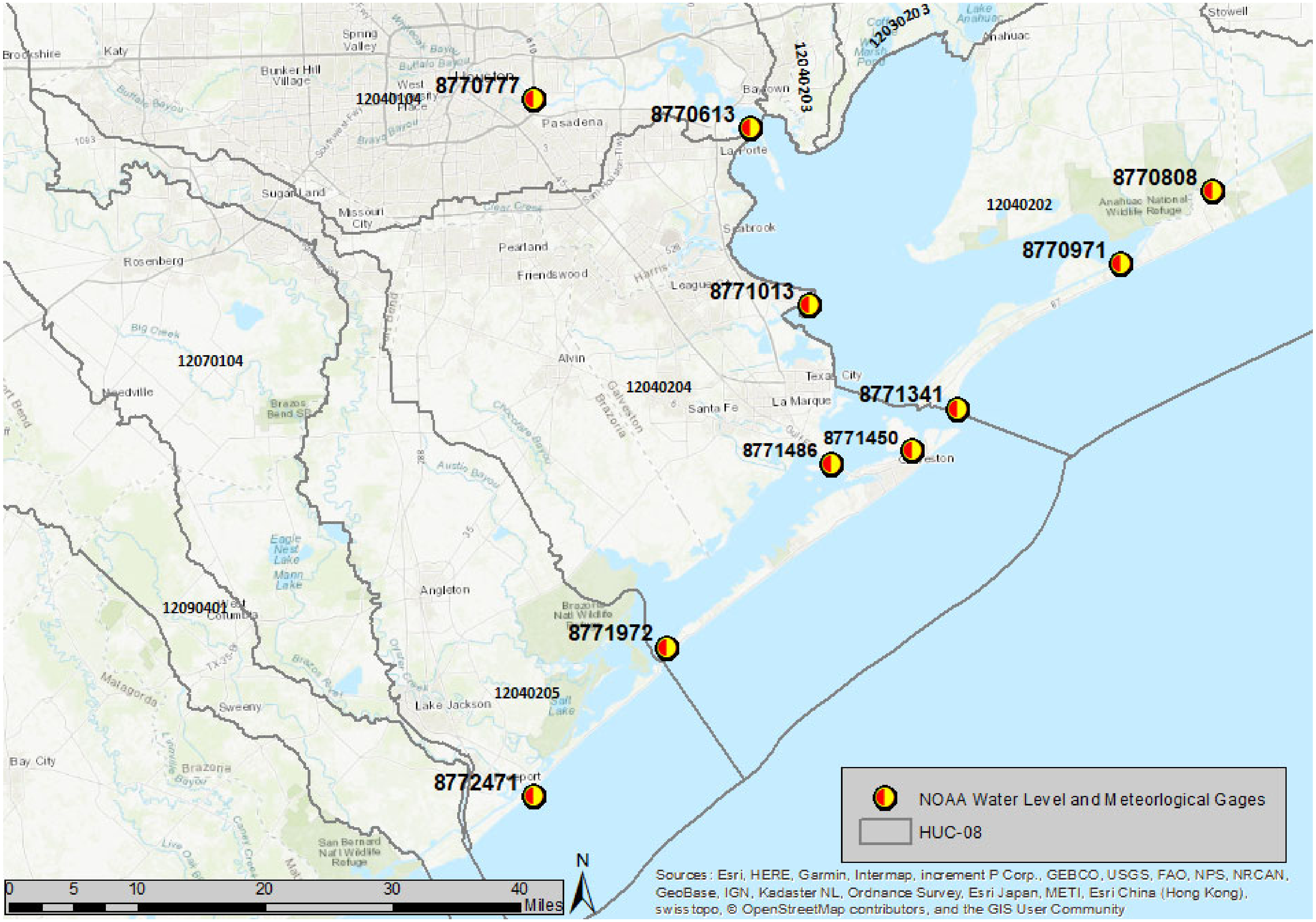

Figure 13: NOAA Tide Gauges near the focus arear of study

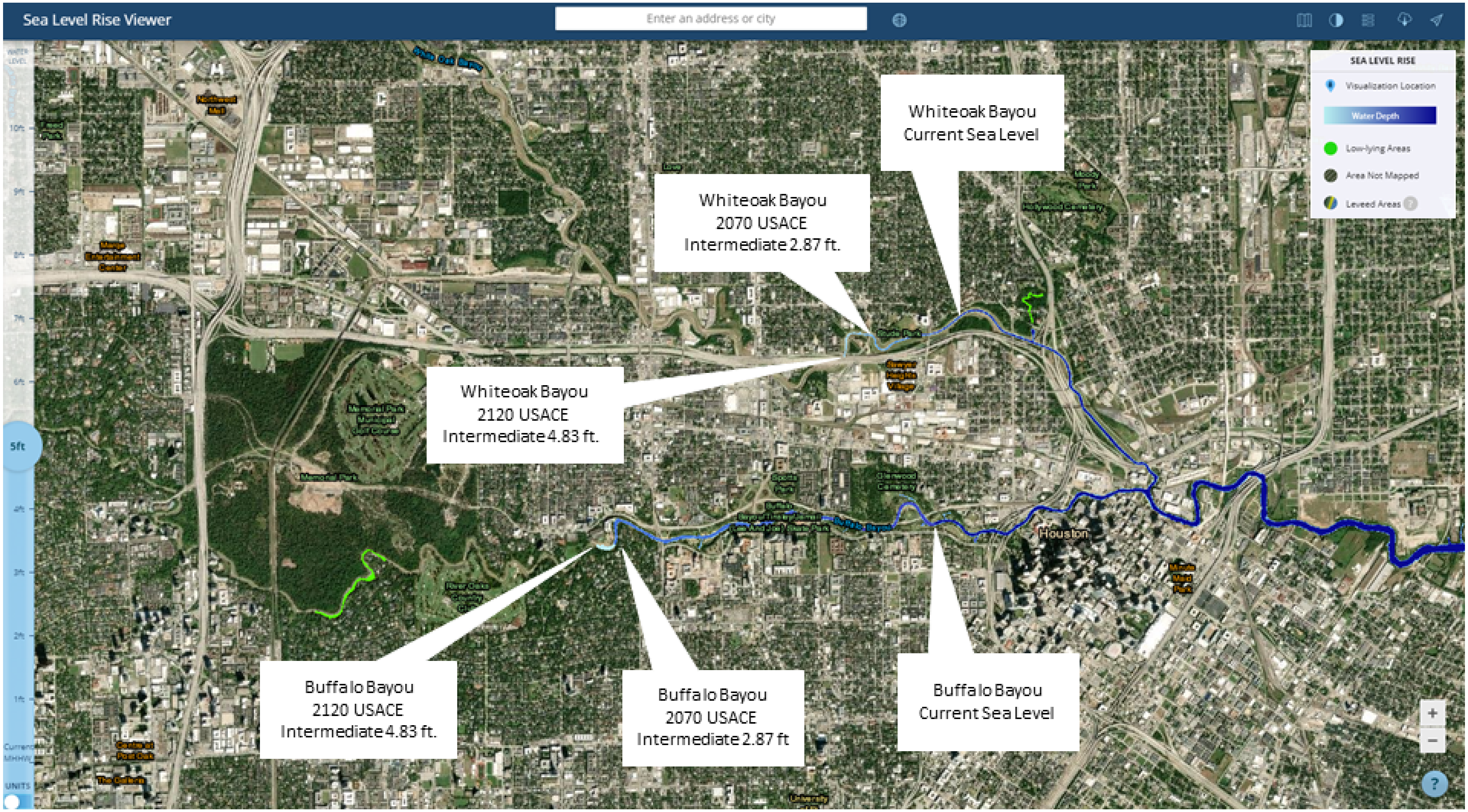

Figure 14: NOAA Sea Level Rise Viewer – Buffalo Bayou and White Oak Bayou

4.4 CLIMATE HYDROLOGY ASSESSMENT: PROJECTED TRENDS IN STREAMFLOW AND CLIMATE CHANGE AT A REGIONAL SCALE

The USACE Climate Hydrology Assessment Tool (CHAT) was used to investigate potential future stream flow trends for HUC 1204 . Figure 15 shows the mean and range of projected annual maximum monthly stream flows computed from 93 different climate change hydrologic model runs for the period of 1950-2099. Global circulation models (GCM) combined with various greenhouse gas emission scenarios create climate changed hydrology outputs to project precipitation and temperature data in the future. The meteorological outputs are spatially downscaled using the Bias Corrected Spatial Downscaling (BCSD) statistical method and then input in the U.S. Bureau of Reclamation's Variable Infiltration Capacity (VIC) precipitation-runoff model to generate streamflow response. The VIC model represents unregulated basin conditions. Based on the model outputs in Figure 15, it can be determined that there is a wide range of projected annual maximum monthly streamflow, and therefore it is difficult to confidently narrow down the most likely future condition scenario. The yellow range in Figure 15 represents the predicted range of annual maximum monthly flow, and the blue line represents the mean predicted annual maximum monthly flow.

Figure 16 shows the result of the CHAT used to determine climate-modeled projected annual maximum monthly flow for HUC 1204 Galveston Bay – San Jacinto. For the period 2000-2099, the average of the 93 Coupled Model Intercomparison Project 5 (CMIP5) climate-changed hydrology model indicates a p-value of 0.0002424 and therefore is statistically significant. The r^2 value is 0.09. The CHAT line of demarcation was set to 1960 due to the region undergoing a significant increase in development at the time.

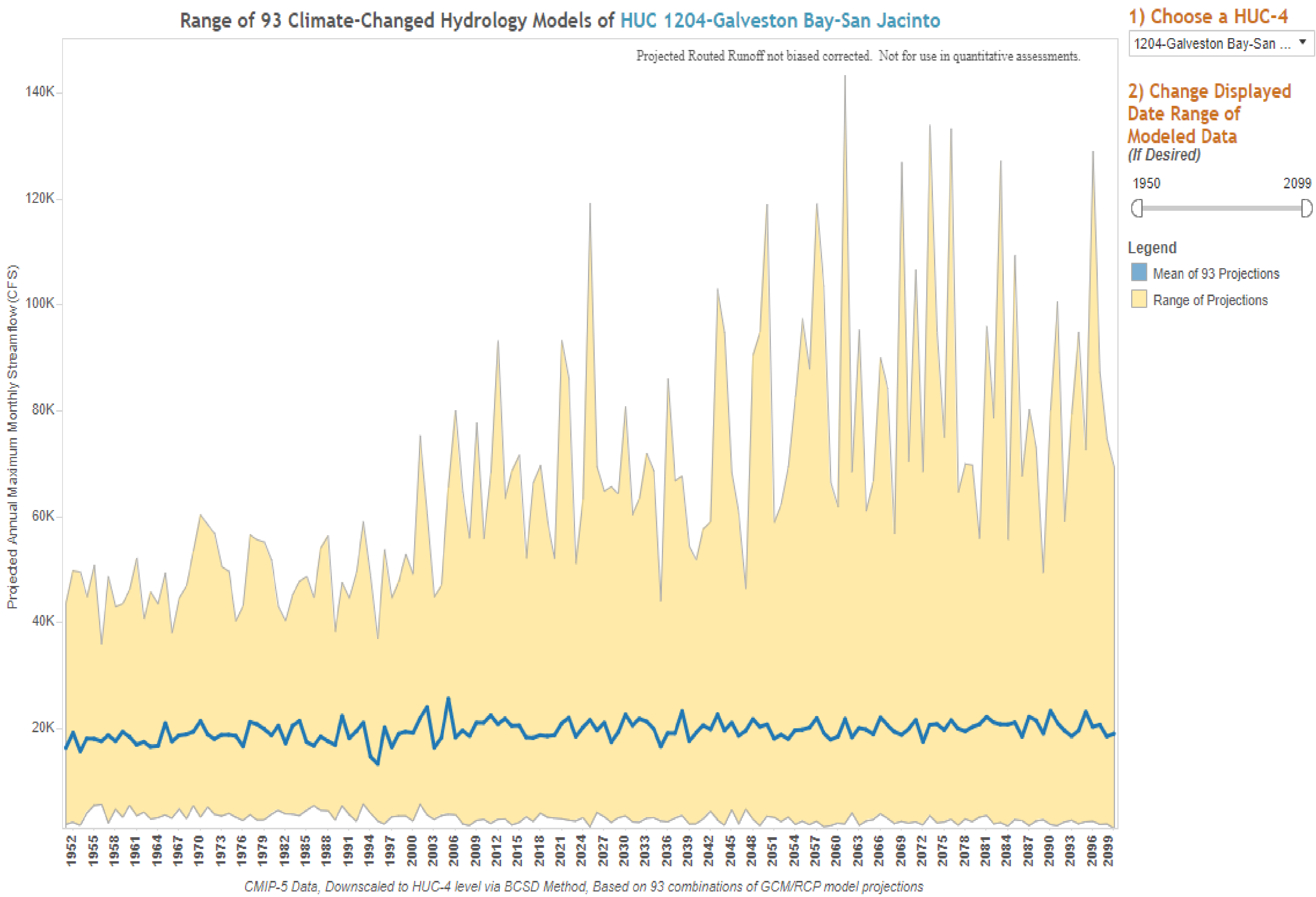

Figure 15: Range of 93 Climate-Changed Hydrology Models of HUC 1204

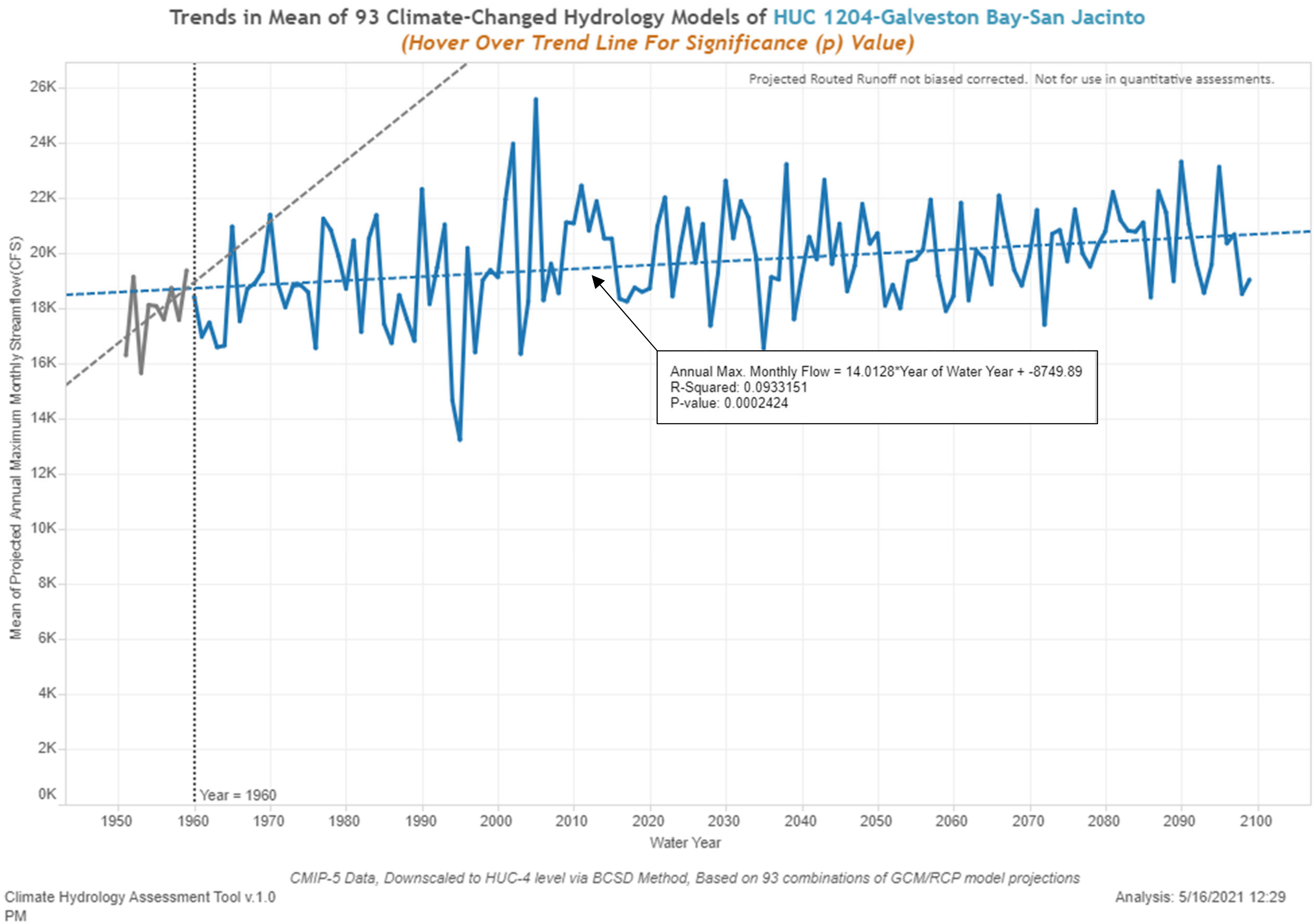

Figure 16 Trends in Mean of 93 Climate-Changed Hydrology Models of HUC 1204

5 VULNERABILITY ASSESSMENT

5.1 SCREENING LEVEL VULNERABILITY ASSESSMENT TO CLIMATE CHANGE IMPACTS

The Vulnerability Assessment Tool (USACE, 2016b) was used to qualitatively characterize flood risk management climate vulnerability in the four-digit HUC 1204 watershed. This tool uses runoff estimated from Global Climate Models (GCM) projections. The GCM projections are divided into two groups. The group with the lower cumulative runoff projections is used to compute values for the dry scenario and the group with the higher runoff projections is used to compute values for the wet scenario. The tool provides results for two of three epochs assessed within the tool:

- 2035-2064 (centered on 2050)
- 2070-2099 (centered on 2085)

The remaining epoch (base period) covers the current time and uses modeled flows generated from the GCM outputs from the base period (1950-1999). Because the base epoch is not based on projections, it is not split into two different scenarios. Eight of the tool's 27 indicators are used to evaluate vulnerability of Metro Houston by analyzing HUC 1204, Galveston Bay-San Jacinto.

The Flood Risk Reduction National Standard default set of indicators was modified to add 156 SEDIMENT, 571L_10PERC_EXCEEDANCE, 571C_10PERC_EXCEEDANCE, 175L_ANNUAL_COV. 277_RUNOFF_PRECIP was removed. Importance weights were adjusted and the ORness factor used was 0.6 rather than the default of 0.7. As sedimentation is an important process related to performance of the existing region and potential proposed recommendations, it was weighted the highest in the group at a factor of 1.8. 590_URBAN_500YR FLOODPLAIN_AREA was weighted 1.75 to better assess the long-term floodplain vulnerability. Table 6 lists the indicator short names, their descriptions and importance weight entered in the Vulnerability Assessment (VA) tool.

Table 6: USACE Screening-Level Climate Change Vulnerability Assessment (VA) Indicators for Flood Risk Reduction Business Line

Indicator Short Name	Indicator Description	Importance Weight
156_SEDIMENT	Change in sediment load due to change in future precipitation (The ratio of the change in the sediment load in the future to the present load.)	1.80

Indicator Short Name	Indicator Description	Importance Weight
568C_FLOOD _MAGNIFICATION	Change in flood runoff: ratio of indicator 571C (monthly runoff exceeded 10% of the time, including upstream freshwater inputs) to 571C in base period.	1.80
568L_FLOOD _MAGNIFICATION	Change in flood runoff: Ratio of indicator 571L (monthly runoff exceeded 10% of the time, excluding upstream freshwater inputs) to 571L in base period.	1.60
175L_ANNUAL_COV	Long-term variability in hydrology: ratio of the standard deviation of annual runoff to the annual runoff mean. Excludes upstream freshwater inputs (local).	1.40
175C_ANNUAL_COV	Long-term variability in hydrology: ratio of the standard deviation of annual runoff to the annual runoff mean. Includes upstream freshwater inputs (cumulative).	1.25
571C_10PERC_EXCEEDANCE	Flood runoff: monthly runoff that is exceeded 10% of the time, including upstream freshwater inputs (cumulative).	1.50
571L_10PERC_EXCEEDANCE	Flood runoff: monthly runoff that is exceeded 10% of the time, excluding upstream freshwater inputs (local).	1.00
590_URBAN_500YR FLOODPLAIN_AREA	Acres of urban area within the 500-year floodplain.	1.75

Weighted order weighted average (WOWA) scores are created for all the indicators, higher values indicate higher vulnerability, and aggregated by base year, two future scenarios (Wet and Dry), over two epochs (2050 and 2085). Results of the vulnerability analysis are presented in Tables 7 through 9.

Table 7: USACE VA analysis results for HUC 1204, Flood Risk Reduction Business Line

	Epoch & Scenario				
Indicator	Base	2050 - Dry	2085 - Dry	2050 - Wet	2085 - Wet
156_SEDIMENT	6.1	2.0	0.0	12.6	20.7
175C_ANNUAL_COV	4.9	7.5	7.3	5.2	5.3
175L_ANNUAL_COV	7.2	11.0	10.7	6.7	6.8
568C_FLOOD_MAGNIFICATION	11.2	9.2	9.0	19.4	15.7
568L_FLOOD_MAGNIFICATION	8.7	6.2	6.1	10.7	10.6
571C_10PERC_EXCEEDANCE	13.0	13.1	13.1	8.7	8.7
571L_10PERC_EXCEEDANCE	20.5	20.6	18.0	19.4	18.1
590_URBAN_500YRFLOODPLAIN_AREA	16.7	17.3	20.7	14.8	13.4

Table 8: USACE VA analysis results for HUC 1204, Flood Risk Reduction Business Line, and Dominant Indicator by Scenario/Epoch

Epoch	Scenario	Dominant Indicator	WOWA Contribution	Total WOWA
Base	N/A	571L_10PERC_EXCEEDANCE	20	88
2085	Dry	590_URBAN_500YRFLOODPLAIN_AREA	21	85
2085	Wet	156_SEDIMENT	21	99
2050	Dry	571L_10PERC_EXCEEDANCE	21	87
2050	Wet	571L_10PERC_EXCEEDANCE	19	97

Table 9: USACE VA analysis results for HUC 1204, Flood Risk Reduction Business Line, and Least Dominant Indicator by Scenario/Epoch

Epoch	Scenario	Least Dominant Indicator	WOWA Contribution	Total WOWA
Base	N/A	175C_ANNUAL_COV	5	88
2085	Dry	156_SEDIMENT	0	85
2085	Wet	175C_ANNUAL_COV	5	99
2050	Dry	156_SEDIMENT	2	87
2050	Wet	175C_ANNUAL_COV	5	97

The results show that the overall watershed vulnerability changes little between the Base (WOWA = 88) and Dry scenario for both 2050 (WOWA =85) and 2085 (WOWA =87) epochs. Vulnerability increases in the Wet scenario with WOWA scores of 97 and 99 for 2050 and 2085 respectively, increases between 10 and 13 %, indicating future performance risk for constructed FRM projects. The dominant indicator driving the vulnerability is 156_SEDIMENT in the Wet scenario, WOWA scores of 12.6 and 20.7 in 2050 and 2085 respectively, a significant increase over the Base condition of 6.1. The 571L_10PERC_EXCEEDANCE indicator is dominant in the 2050 Wet scenario and is a significant contributor to the overall performance score. When combined with 156_SEDIMENT, WOWA scores are BASE = 26.6, DRY 2050 = 22.6, DRY 2085 = 18.0, WET 2050 = 32, WET 2085 = 38.8. The most significant difference is between the future 2085 Dry/Wet scenarios 38.8 versus 18.0.

6 SUMMARY

Threats to the Metro Houston area and regional resilience generally take two forms: acute shocks (e.g., heavy rain events, hurricanes) and chronic stressors (e.g., climate change, aging infrastructure). Focusing on FRM efforts in the region the two most significant climactic impacts are associated with RSLC and precipitation extremes. Annual rainfall projections are an important consideration for water resources issues such as water supply and environmental flows to Galveston Bay, though are not a substantial consideration for FRM. Wetter precipitation extremes and increasing RSLC are both detrimental future conditions for FRM efforts in the region.

Increasing RSLC degrades conveyance in the tidally-impacted portions of coastal watersheds. Though many areas may not feel “coastal” in the same way as Galveston or Clear Lake, the tidal influence in Houston watersheds propagates well inland (fig. 14 and attachment 2). This is an obvious concern for the Houston regional exposure to hurricane surge and other tropical events, but RSLC will also impact rainfall runoff inundation not associated with tropical events.

Separate from the RSLC issues, though with the potential to exacerbate flooding issues, is the potential for wetter extreme precipitation events. FRM infrastructure design is based on intensity-duration-frequency relationships which are available from NOAA Atlas 14 (Perica et al., 2018). The rainfall intensity and depths for a given duration and frequency increased from the prior relationships. Further changes in extreme precipitation could impact infrastructure that was designed and constructed prior to updates. There remains some uncertainty the projected magnitude of future changes which is an opportunity for future investigation.

The long-term implications for climate change are important to consider during projects to ensure the features are resilient to the envelope of likely future conditions.

7 REFERENCES

Bawden, G.W., Johnson, M.R., Kasmarek, M.C., Brandt, Justin, and Middleton, C.S. (2012). *Investigation of land subsidence in the Houston-Galveston region of Texas by using the Global Positioning System and interferometric synthetic aperture radar, 1993–2000: U.S. Geological Survey Scientific Investigations Report*

Dai, A., T. Zhao, and J. Chen (2018). *Climate Change and Drought: a Precipitation and Evaporation Perspective. Current Climate Change Reports*

Climate Hydrology Assessment Tool. (2015). https://corpsmapz.usace.army.mil/apex/f?p=313:2:0::NO:::

Easterling, D.R., K.E. Kunkel, J.R. Arnold, T. Knutson, A.N. LeGrande, L.R. Leung, R.S. Vose, D.E. Waliser, and M.F. Wehner (2017). *Precipitation change in the United States. Climate Science Special Report: Fourth National Climate Assessment, Volume I*

Engineering and Construction Bulletins. (2018). *Engineering and Construction Bulletin 2018-14: Guidance for Incorporating Climate Change Impacts to Inland Hydrology in Civil Works Studies, Designs, and Projects*

Engineer Regulation. (2013). *Engineering Regulation 1100-2-8162: Incorporating Sea Level Change in Civil Works Programs*

Grundstein A, Dowd J. (2011). *Trends in extreme apparent temperatures over the United States*

Houston-Galveston Area of Council (H-GAC). (2018). *Houston-Galveston Area Council - Regional Growth Forecast.* Retreived from http://www.h-gac.com/regional-growth-forecast/default.aspx

Highfield, W.E., Brody, S.D., Atoba K., and Blessing R. (2017). *Identifying the Future Costs of Flooding in the Houston-Galveston Region*

Neilson-Gammon, J. (2018). *Seeking the New Abnormal*

Kunkel KE, Liang X-Z, Zhu J. (2010). *Regional climate model projections and uncertainties of U.S. summer heat waves*

Kunkel KE, Stevens S, Sun L, Janssen E, Wuebbles D, Kruk MC, Thomas DP, Shulski MD, Umphlett N, Hubbard KG, Robbins K, Romolo L, Akyuz A, Pathak T, Bergantino TR, Dobson JG (eds.). (2013). *Regional Climate Trends and Scenarios for the U.S. National Climate Assessment: Part 4. Climate of the U.S. Great Plains*

Letetrel, C., M. Karpytchev, M. N. Bouin, M. Marcos, A. SantamarÍa-Gómez, and G. Wöppelmann. (2015). *Estimation of vertical land movement rates along the coasts of the Gulf of Mexico over the past decades*

Liu Y, Goodrick SL, Stanturf JA. (2013). *Future U.S. wildfire potential trends projected using a dynamically downscaled climate change scenario*

McRoberts DB, Nielsen-Gammon JW. (2011). *A new homogenized climate division precipitation dataset for analysis of climate variability and climate change*

Nonstationarity Detection Tool. (2016) http://ec2-34-205-128-255.compute-1.amazonaws.com:8080/tst_app/#shiny-tab-upload_home

Paine, J.G., Caudle T.L., and Andrews J.R. (2017): *Shoreline and sand storage dynamics from annual airborne LIDAR surveys, Texas Gulf Coast*

Palecki MA, Angel JR, Hollinger SE. (2005). *Storm precipitation in the United States. Part I: Meteorological characteristics*

Perica, S, Pavlovic, S, St. Laurent, M, Trypaluk, C, Unruh, D, Wilhite, O. (2018). *NOAA Atlas 14 Precipitation-Frequency Atlas of the United States, Volume 11 Version 2.0: Texas*

PRISM Climate Group. (2010). PRISM Climate Data. Retreived from http://prism.oregonstate.edu

Runkle, J., Kunkel K., Nielsen-Gammon J.,. Frankson R, Champion S., Stewart B., Romolo L., and Sweet W. (2017). *Texas State Climate Summary*

Sea Level Change Curve Calculator. (2014). https://cwbi-app.sec.usace.army.mil/rccslc/slcc_calc.html

Scherer M, Diffenbaugh N. (2014). *Transient twenty-first century changes in daily-scale temperature extremes in the United States*

Stoner A, Hayhoe K. (2020). *Climate Impact Assessment for the City of Houston*

Tewari, S. (2019). *Combined Effect of Sea-Level Rise and Coastal Land Subsidence - Identification of Critical Transportation Infrastructure At-Risk in Coastal Sptc. Region, Part 2 - Coastal Texas*

Texas A&M University. (2018). *Eye of the Storm: Report of the Governor's Commission to Rebuild Texas*

Texas A&M University. (2020). *Assessment of Historic and Future Trends of Extreme Weather in Texas, 1900-2036*

U.S. Army Corps of Engineers. (2015). *Recent US Climate Change and Hydrology Literature Applicable to U.S. Army Corps of Engineers Missions – Texas-Gulf Region 12*

U.S. Army Corps of Engineers (2019). *Time Series Toolbox User Guide, Version 1.0*

U.S. Global Change Research Program. (2018). *Southern Great Plains. Impacts, Risks, and Adaptation in the United States: Fourth National Climate Assessment, Volume II*

van Oldenborgh, G.J., van der Wiel, K., Sebastian, A., Singh, R., Arrighi, J., Otto, F., Haustein, K., Li, S., Vecchi, G., Cullen, H. (2018). *Attribution of extreme rainfail from Hurricane Harvey, August 2017*

Vulnerability Assessment Tool. (2015). https://maps.crrel.usace.army.mil/apex/f?p=201:1:

ATTACHMENT 1
Timeseries Toolbox Tool Plots
Metro Houston Regional Watershed Assessment

Attachment 1 consists of the Timeseries Toolbox Plots for all sets of data analzed that had nonstsationarities detected for the Metro Houston Regional Watershed Climate Assessment.

List of Figures

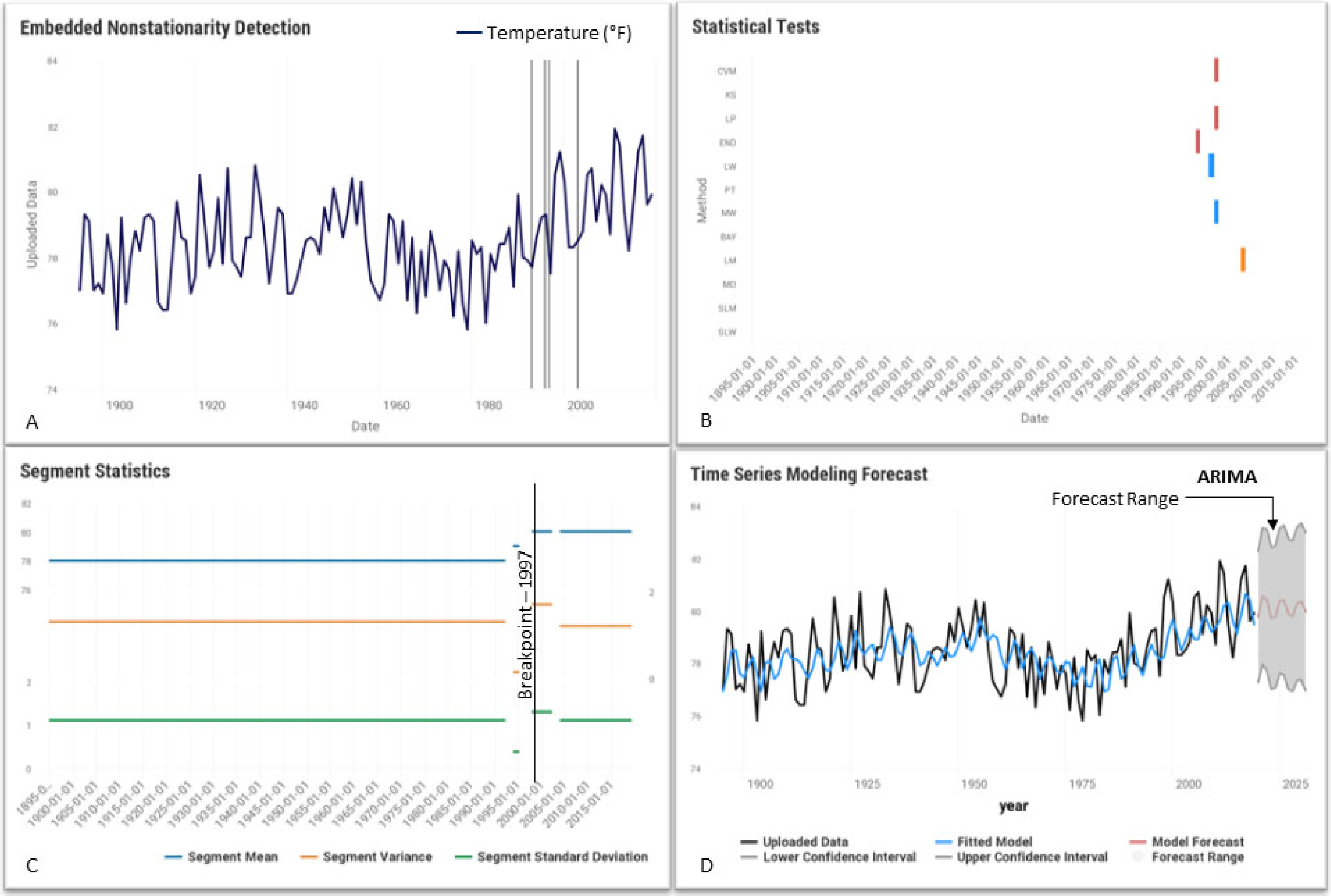

Graph A: Nonstationarity Detection over the analyzed time frame. Graph B: Statistical tests that detected nonstationarity over the analyzed time frame. Graph C: Mean, Variance, Standard Deviation changes over time after nonstationarity detections. Graph D: ARIMA forecast of potential trend in time.

Figure 1 Harris County Temperature Timeseries Toolbox Plots

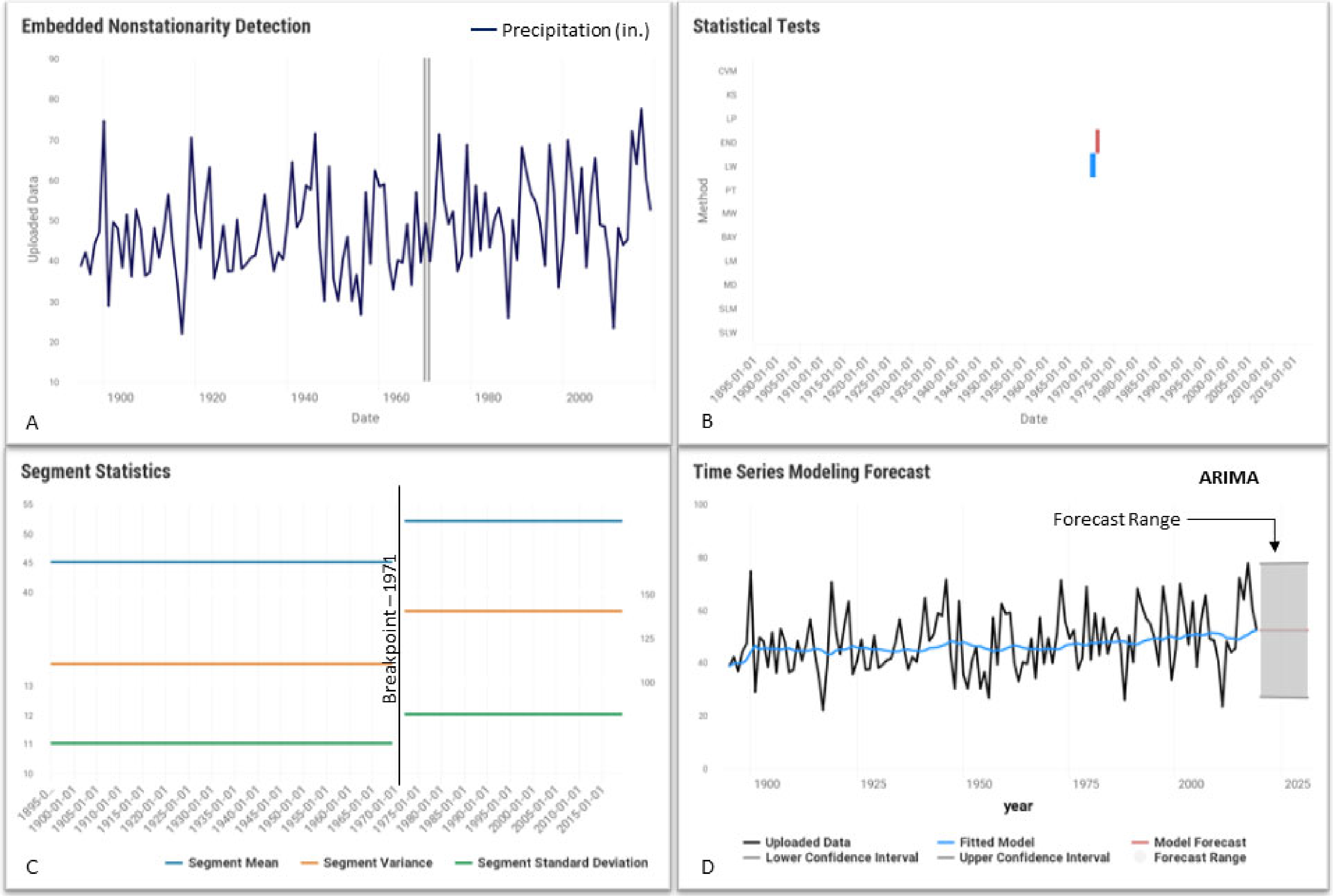

Graph A: Nonstationarity Detection over the analyzed time frame. Graph B: Statistical tests that detected nonstationarity over the analyzed time frame. Graph C: Mean, Variance, Standard Deviation changes over time after nonstationarity detections. Graph D: ARIMA forecast of potential trend in time.

Figure 2 Harris Count Precipitation Timeseries Toolbox Plots

Graph A: Nonstationarity Detection over the analyzed time frame. Graph B: Statistical tests that detected nonstationarity over the analyzed time frame. Graph C: Mean, Variance, Standard Deviation changes over time after nonstationarity detections. Graph D: ARIMA forecast of potential trend in time.

Figure 3 Goose Creek 08067525 Timeseries Toolbox Plots

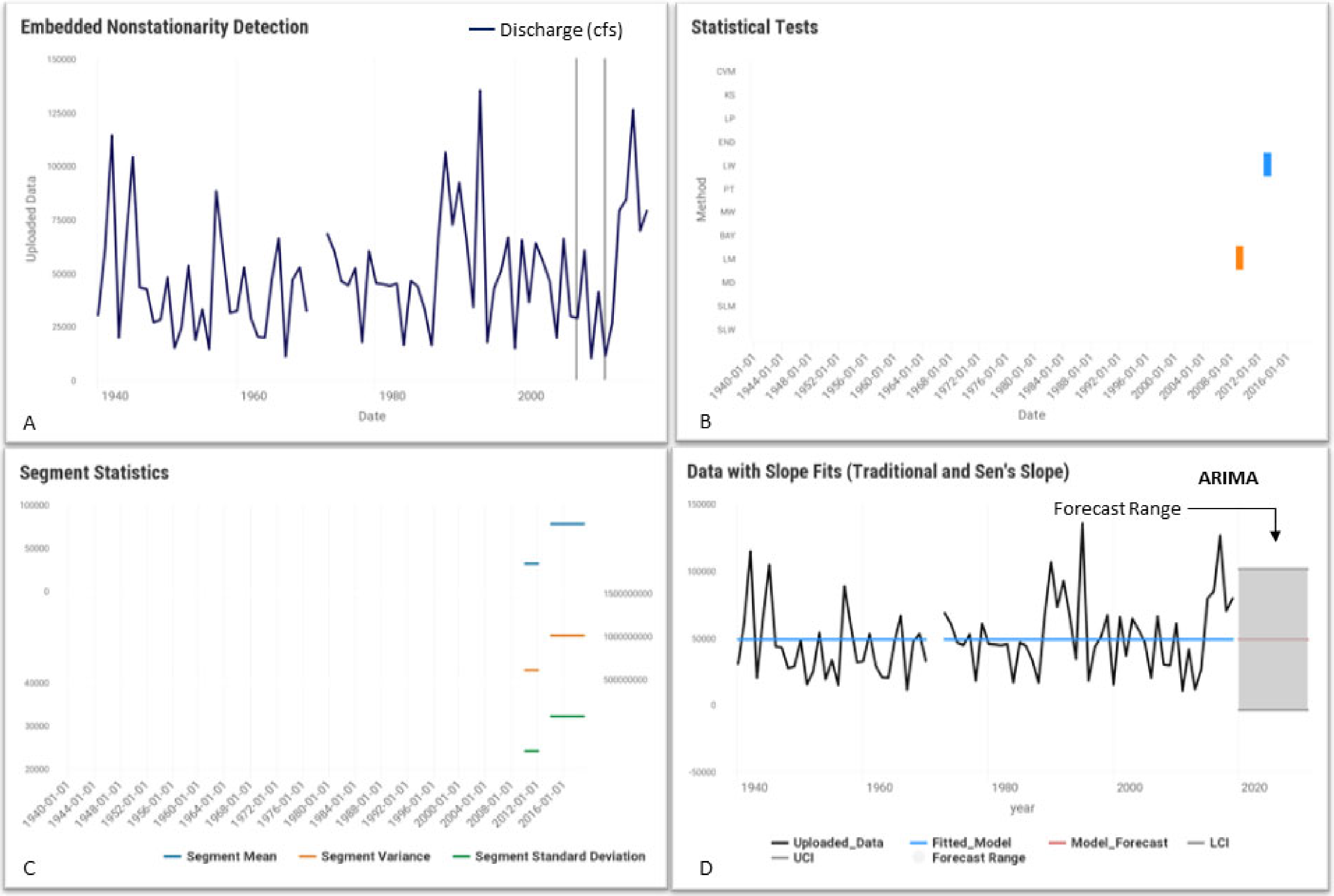

Graph A: Nonstationarity Detection over the analyzed time frame. Graph B: Statistical tests that detected nonstationarity over the analyzed time frame. Graph C: Mean, Variance, Standard Deviation changes over time after nonstationarity detections. Graph D: ARIMA forecast of potential trend in time.

Figure 4 Trinity River 08067000 Timeseries Toolbox Plots

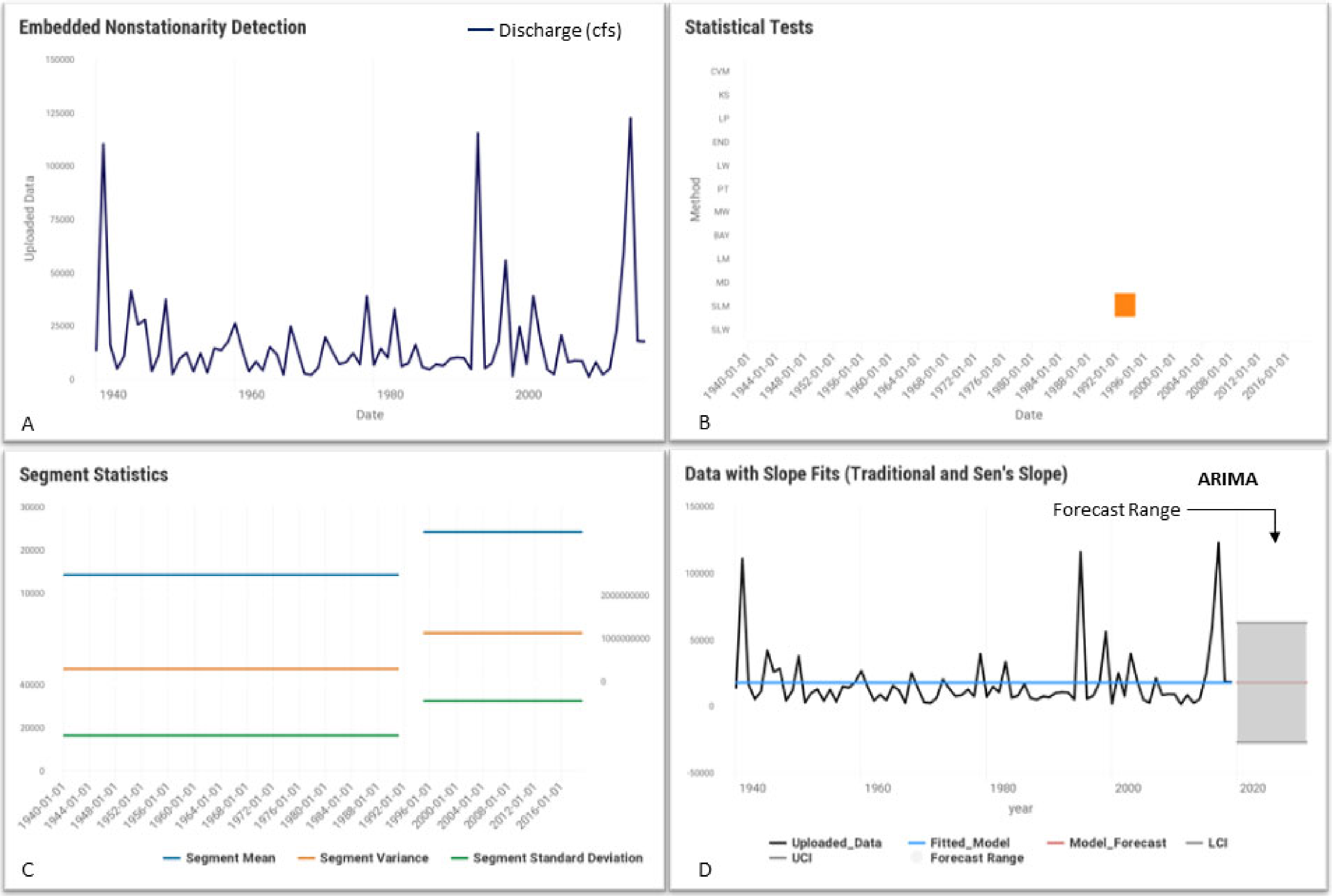

Graph A: Nonstationarity Detection over the analyzed time frame. Graph B: Statistical tests that detected nonstationarity over the analyzed time frame. Graph C: Mean, Variance, Standard Deviation changes over time after nonstationarity detections. Graph D: ARIMA forecast of potential trend in time.

Figure 5 West Fork San Jacinto 08068000 Timeseries Toolbox Plots

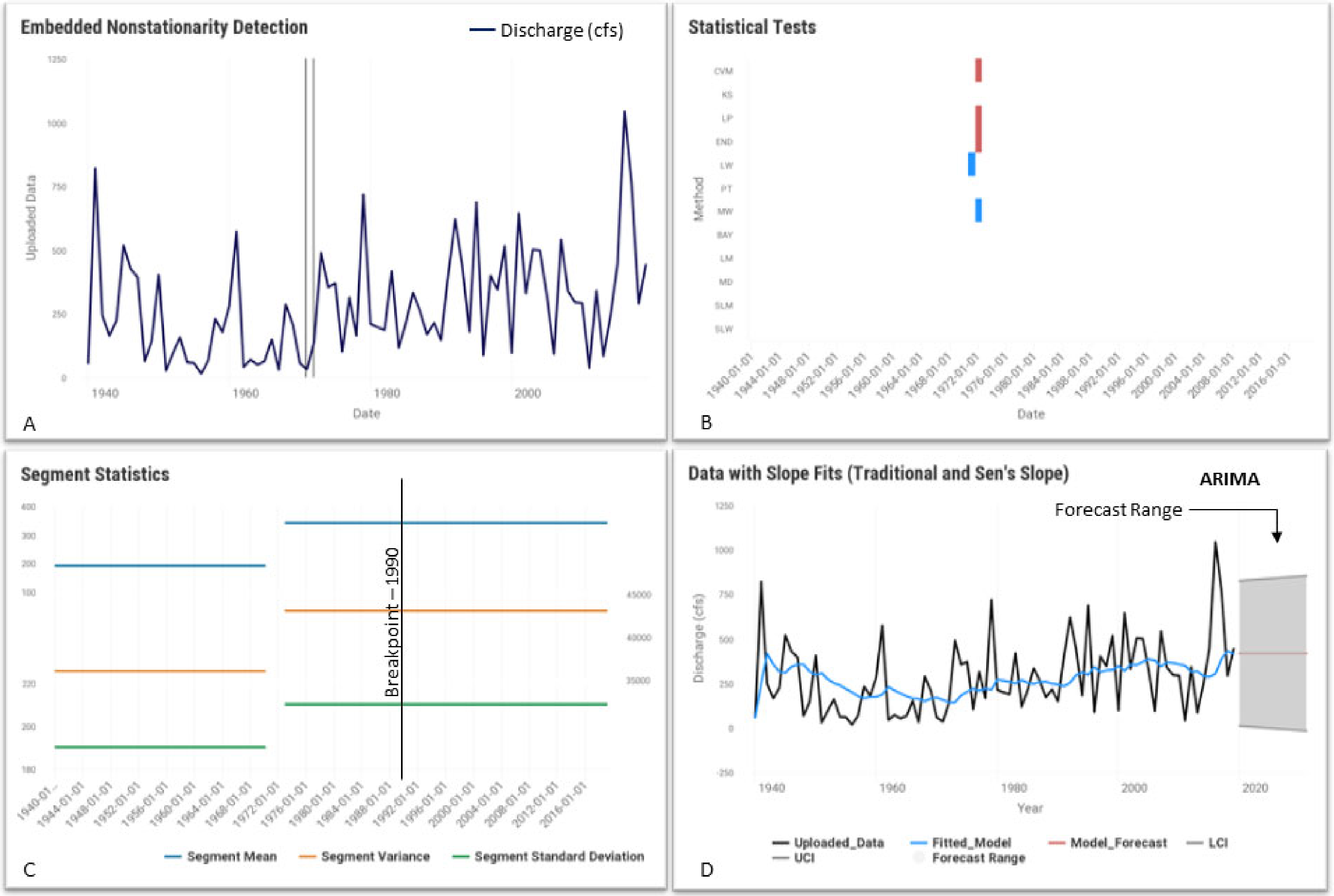

Graph A: Nonstationarity Detection over the analyzed time frame. Graph B: Statistical tests that detected nonstationarity over the analyzed time frame. Graph C: Mean, Variance, Standard Deviation changes over time after nonstationarity detections. Graph D: ARIMA forecast of potential trend in time.

Figure 6 Spring Creek 08068500 Timeseries Toolbox Plots

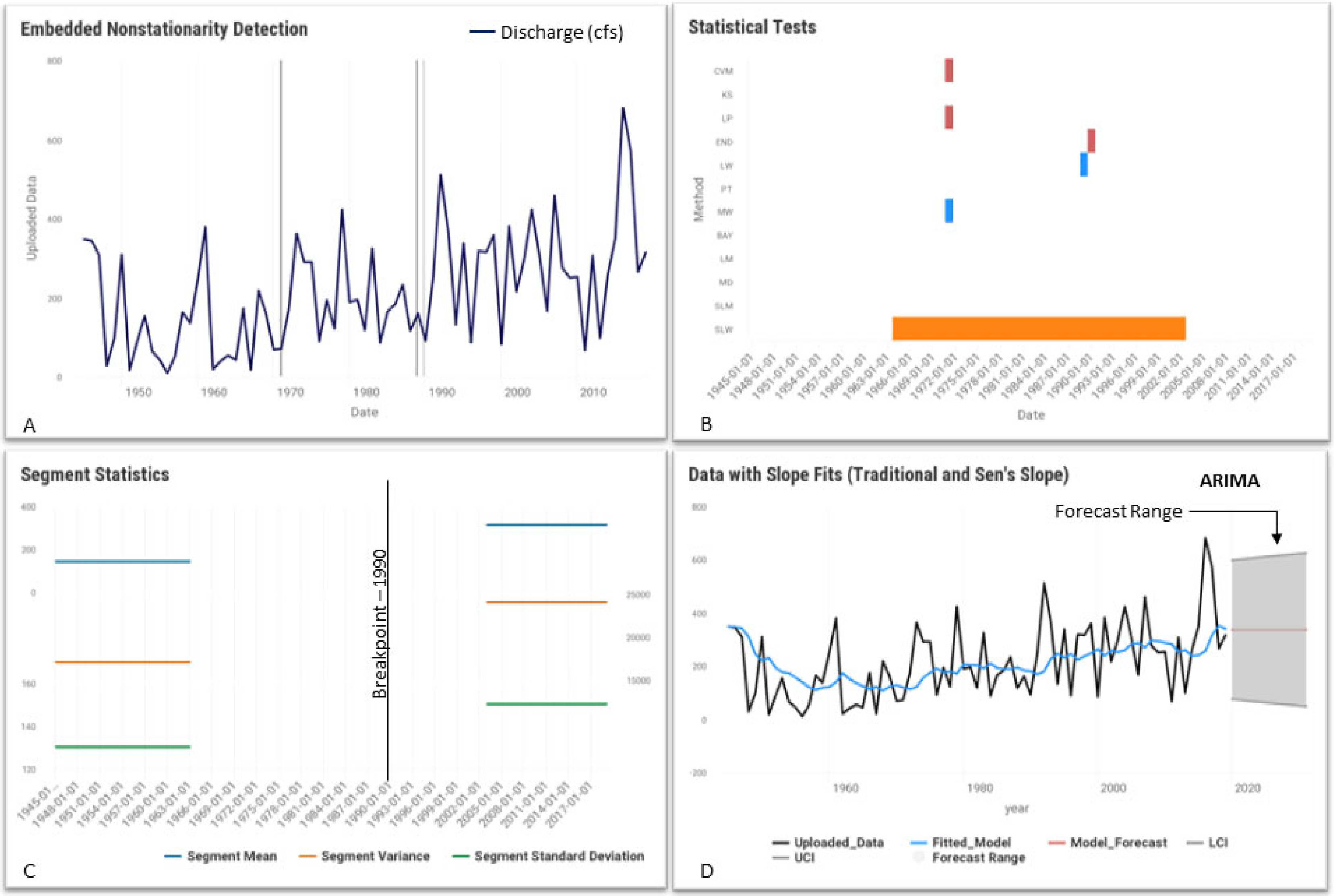

Graph A: Nonstationarity Detection over the analyzed time frame. Graph B: Statistical tests that detected nonstationarity over the analyzed time frame. Graph C: Mean, Variance, Standard Deviation changes over time after nonstationarity detections. Graph D: ARIMA forecast of potential trend in time.

Figure 7 Cypress Creek 08069000 Timeseries Toolbox Plots

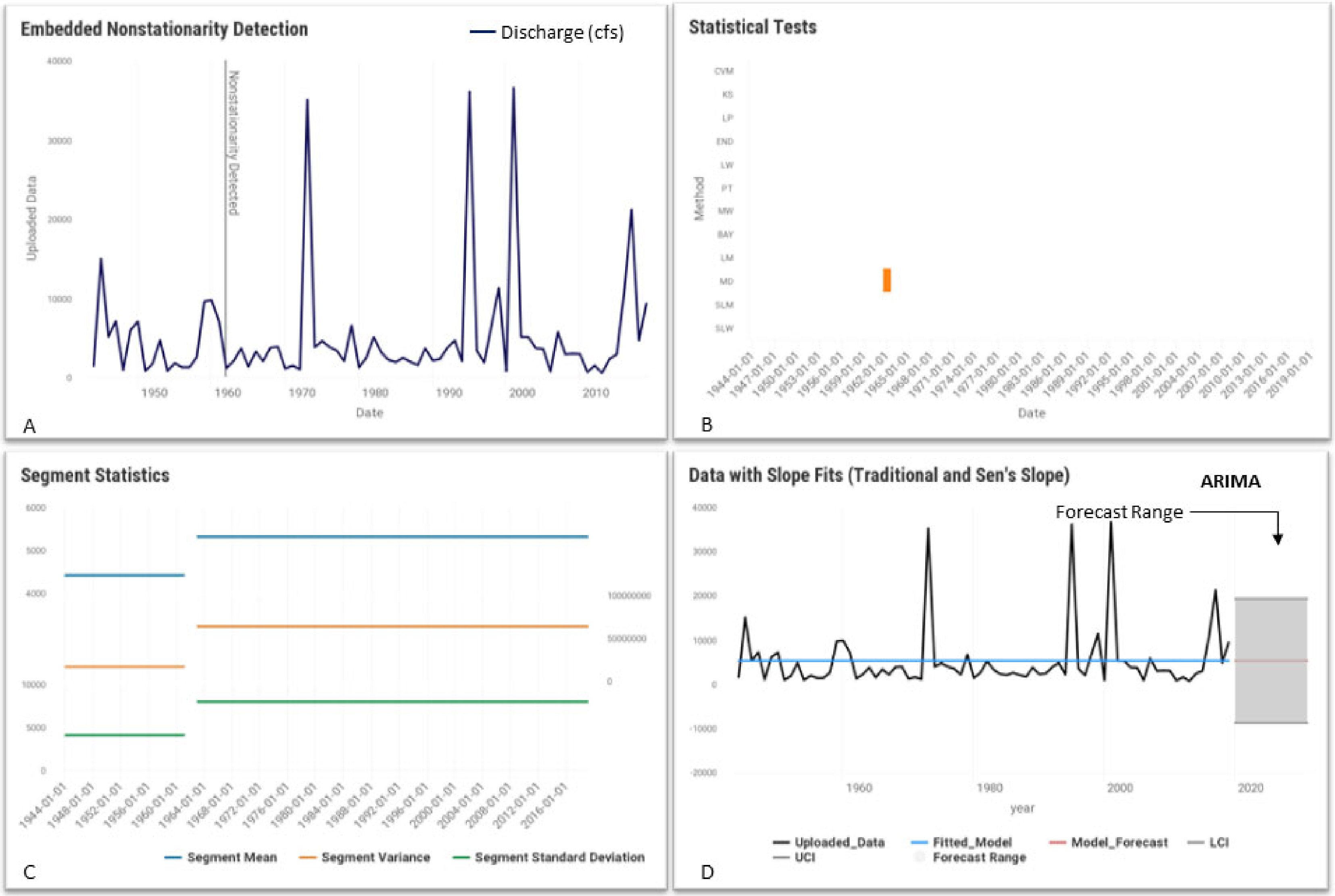

Graph A: Nonstationarity Detection over the analyzed time frame. Graph B: Statistical tests that detected nonstationarity over the analyzed time frame. Graph C: Mean, Variance, Standard Deviation changes over time after nonstationarity detections. Graph D: ARIMA forecast of potential trend in time.

Figure 8 Caney Creek 08070500 Timeseries Toolbox Plots

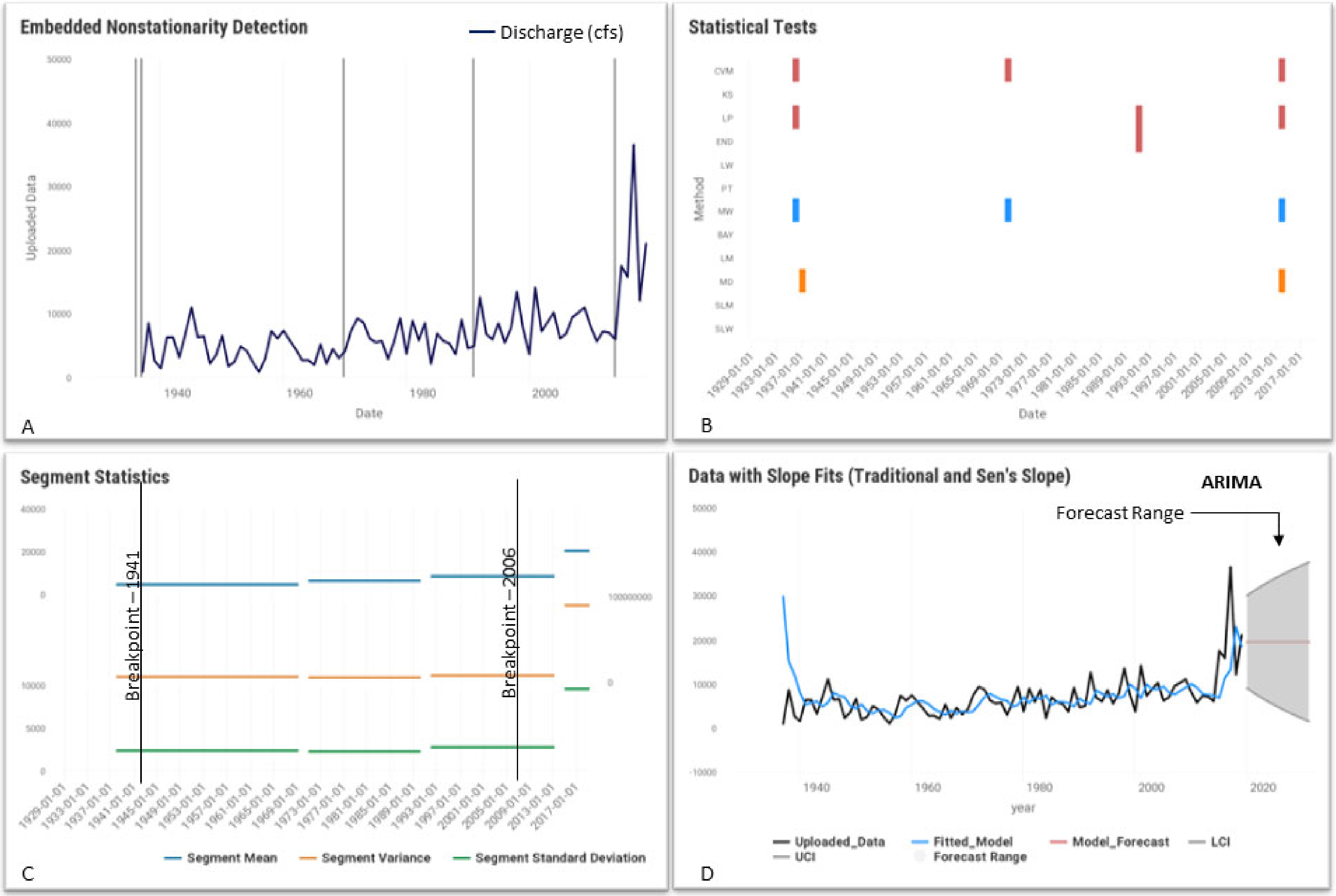

Graph A: Nonstationarity Detection over the analyzed time frame. Graph B: Statistical tests that detected nonstationarity over the analyzed time frame. Graph C: Mean, Variance, Standard Deviation changes over time after nonstationarity detections. Graph D: ARIMA forecast of potential trend in time.

Figure 9 Buffalo Bayou 08074000 Timeseries Toolbox Plots

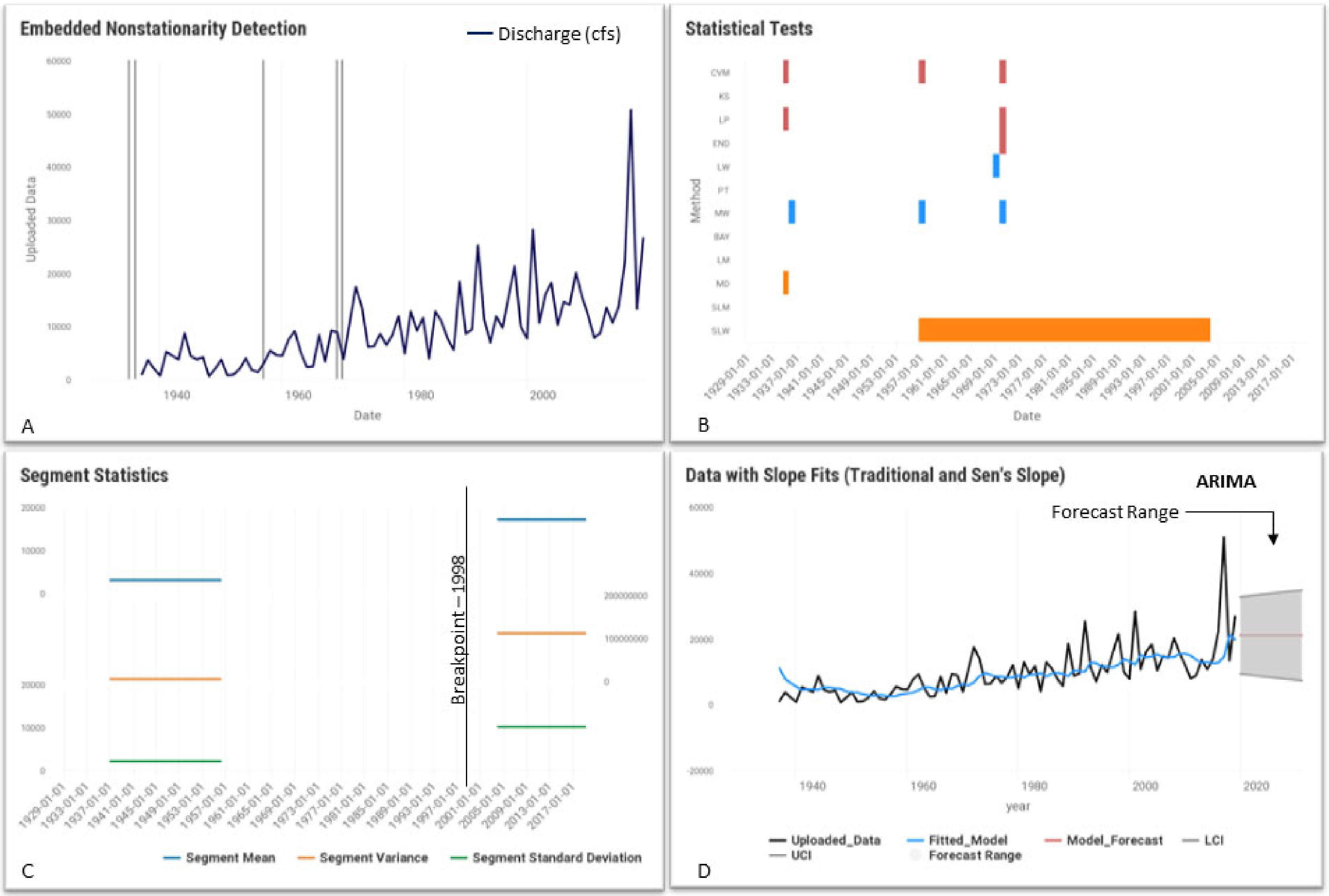

Graph A: Nonstationarity Detection over the analyzed time frame. Graph B: Statistical tests that detected nonstationarity over the analyzed time frame. Graph C: Mean, Variance, Standard Deviation changes over time after nonstationarity detections. Graph D: ARIMA forecast of potential trend in time.

Figure 10 Whiteoak Bayou 08074500 Timeseries Toolbox Plots

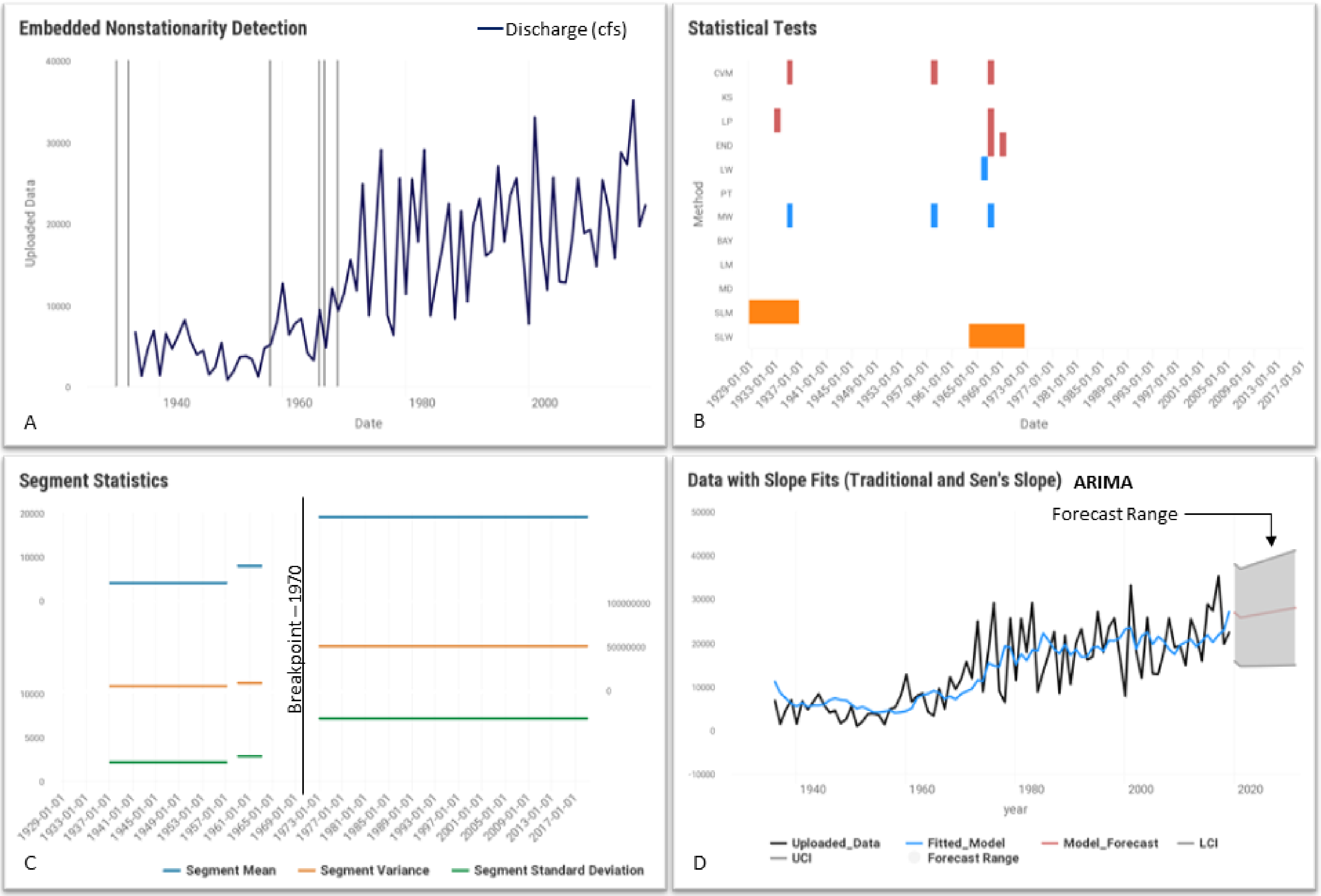

Graph A: Nonstationarity Detection over the analyzed time frame. Graph B: Statistical tests that detected nonstationarity over the analyzed time frame. Graph C: Mean, Variance, Standard Deviation changes over time after nonstationarity detections. Graph D: ARIMA forecast of potential trend in time.

Figure 11 Brays Bayou 08075000 Timeseries Toolbox Plots

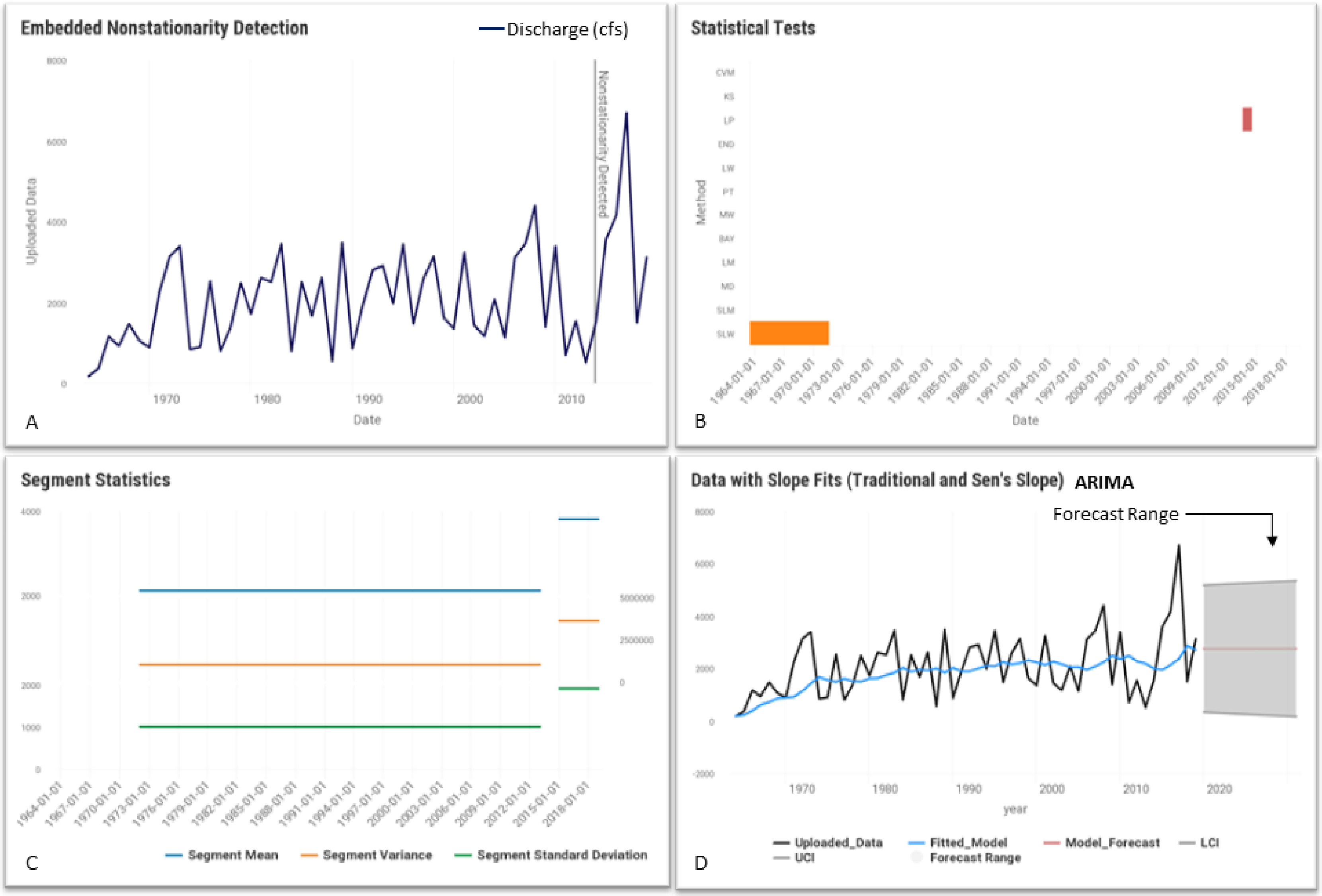

Graph A: Nonstationarity Detection over the analyzed time frame. Graph B: Statistical tests that detected nonstationarity over the analyzed time frame. Graph C: Mean, Variance, Standard Deviation changes over time after nonstationarity detections. Graph D: ARIMA forecast of potential trend in time.

Figure 12 Hunting Bayou 08075770 Timeseries Toolbox Plots

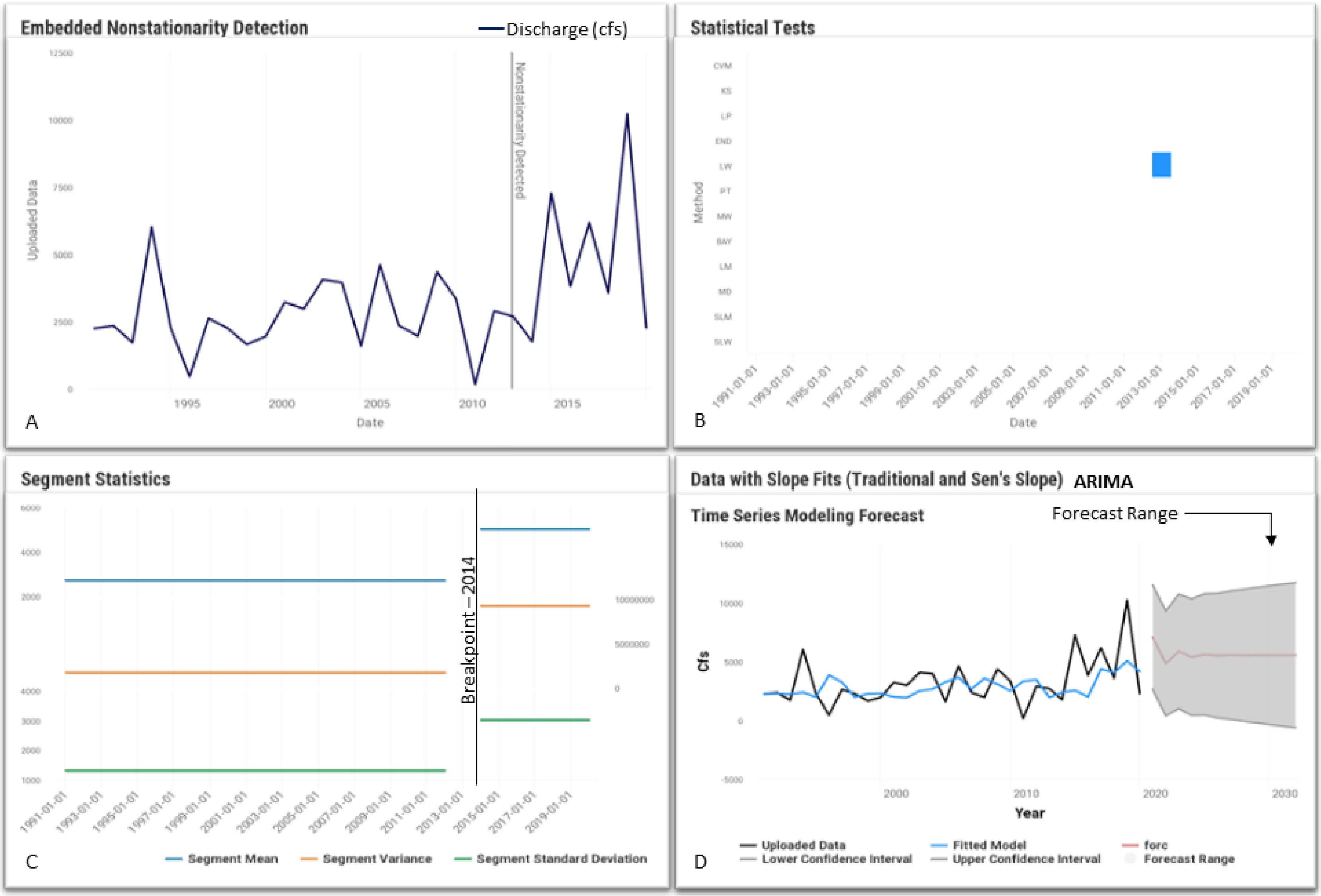

Graph A: Nonstationarity Detection over the analyzed time frame. Graph B: Statistical tests that detected nonstationarity over the analyzed time frame. Graph C: Mean, Variance, Standard Deviation changes over time after nonstationarity detections. Graph D: ARIMA forecast of potential trend in time.

Figure 13 Big Creek 08115000 Timeseries Toolbox Plots

Attachment 2
NOAA Sea Level Rise Viewer for Coastal Watersheds
Metropolitan Houston Regional Watershed Area

Attachment 2 consists of the NOAA Sea Level Rise Viewer for some of the major waterways within coastal watersheds for the Metro Houston Regional Watershed Climate Assessment.

List of Figures

Attachment 2
NOAA Sea Level Rise Viewer for Coastal Watersheds
Metropolitan Houston Regional Watershed Area

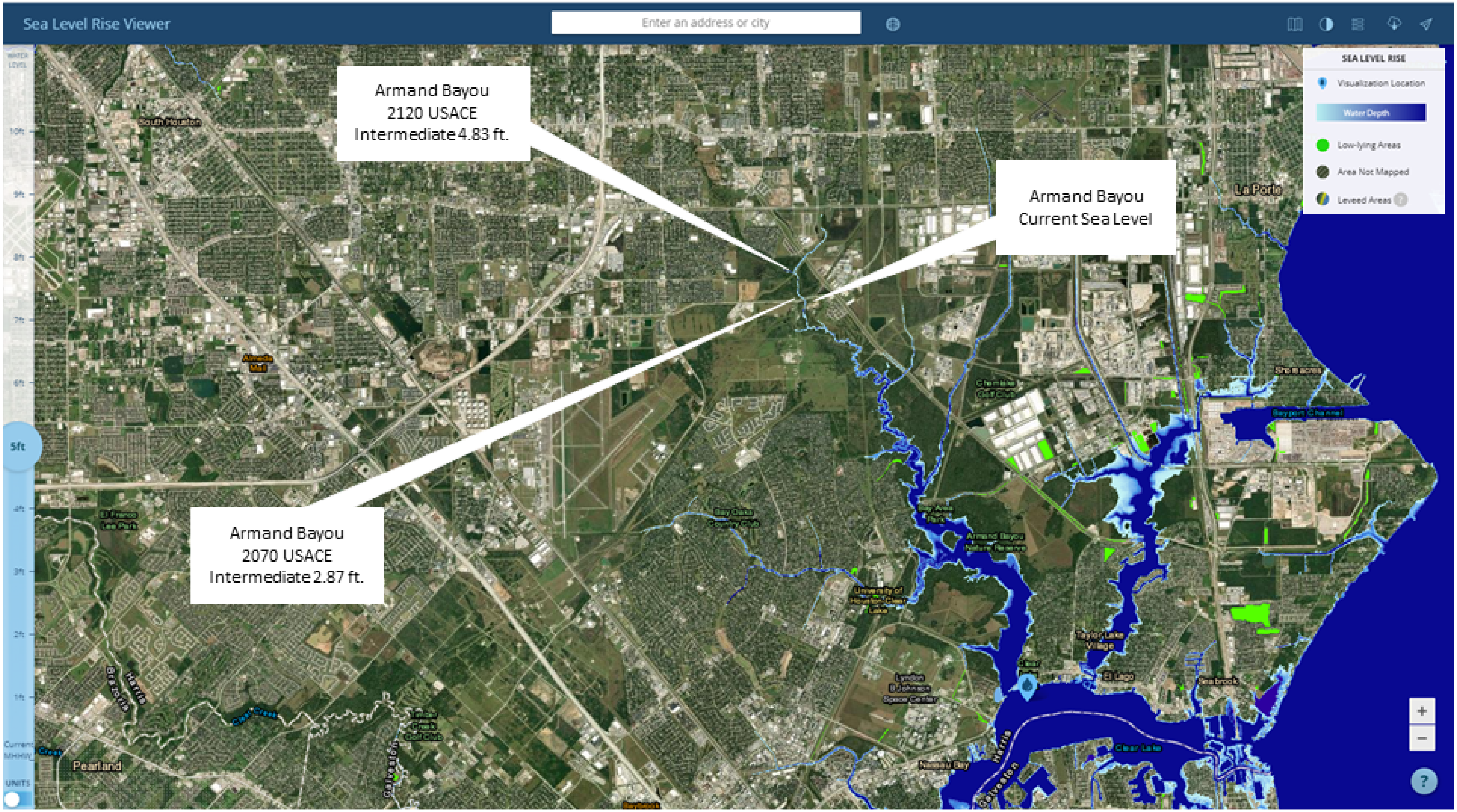

Figure 1 NOAA Sea Level Rise Viewer - Armand Bayou

Attachment 2
NOAA Sea Level Rise Viewer for Coastal Watersheds
Metropolitan Houston Regional Watershed Area

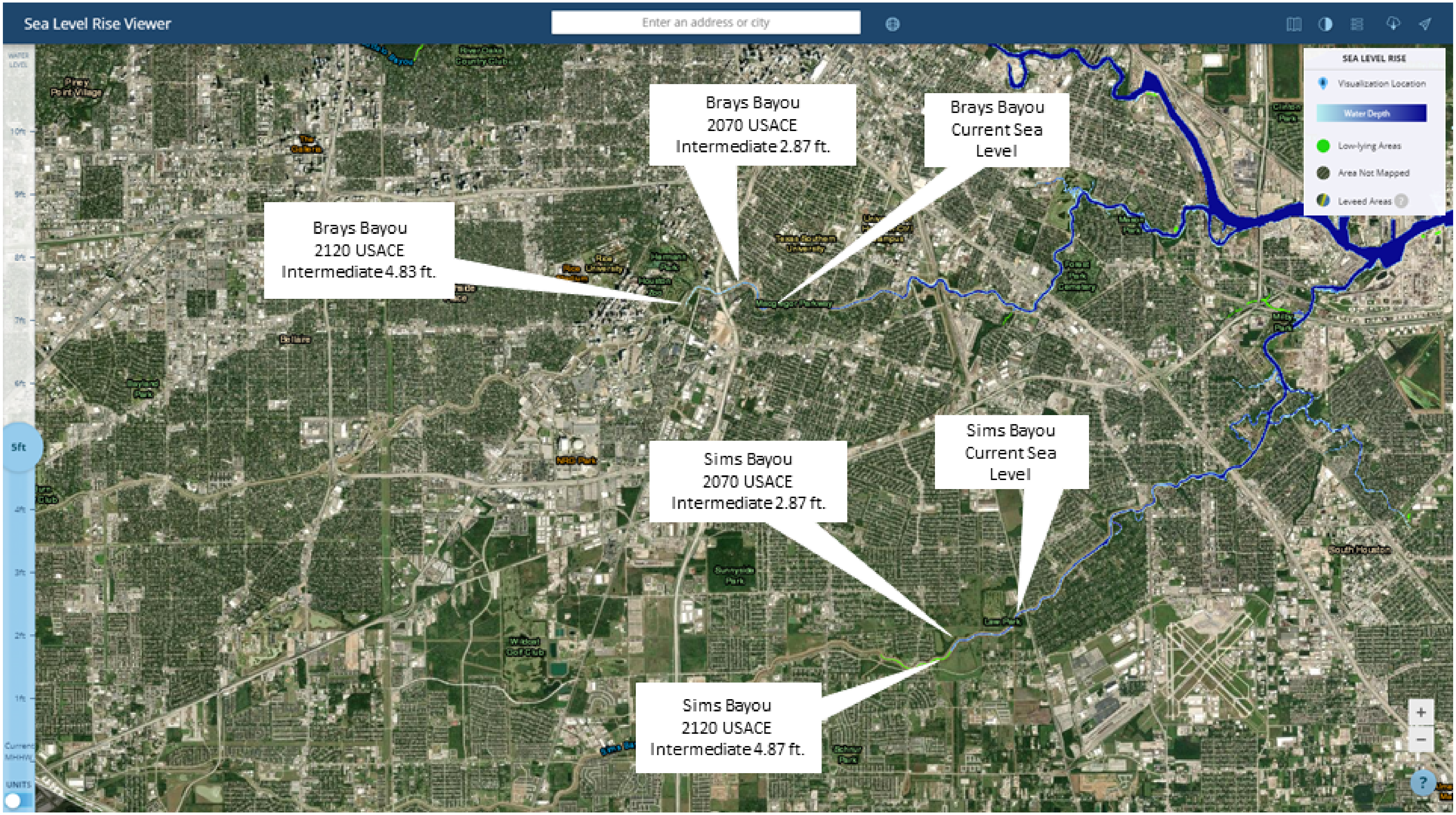

Figure 2 NOAA Sea Level Rise Viewer - Brays Bayou and Whiteoak Bayou

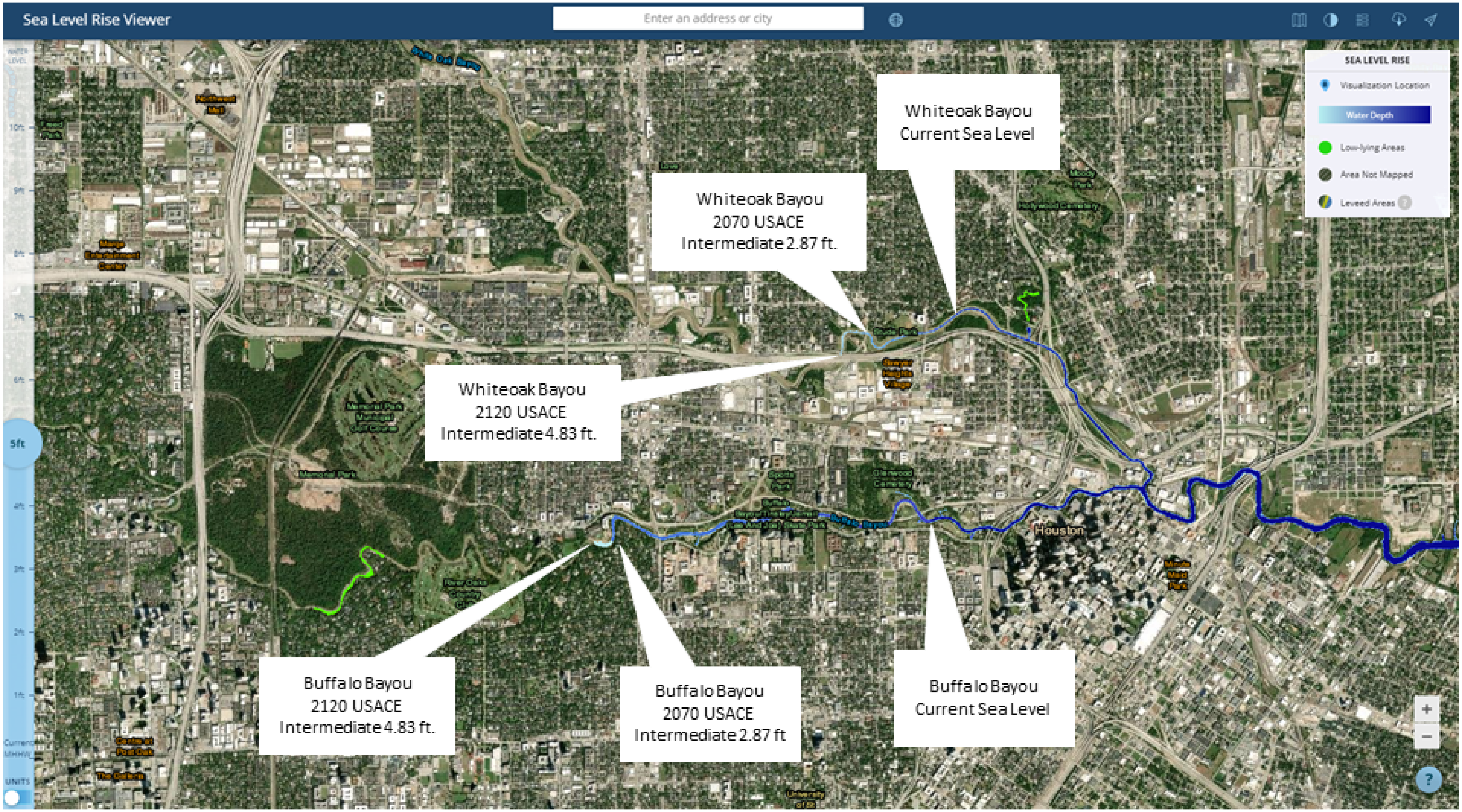

Figure 3 NOAA Sea Level Rise Viewer - Buffalo Bayou and Sims Bayou

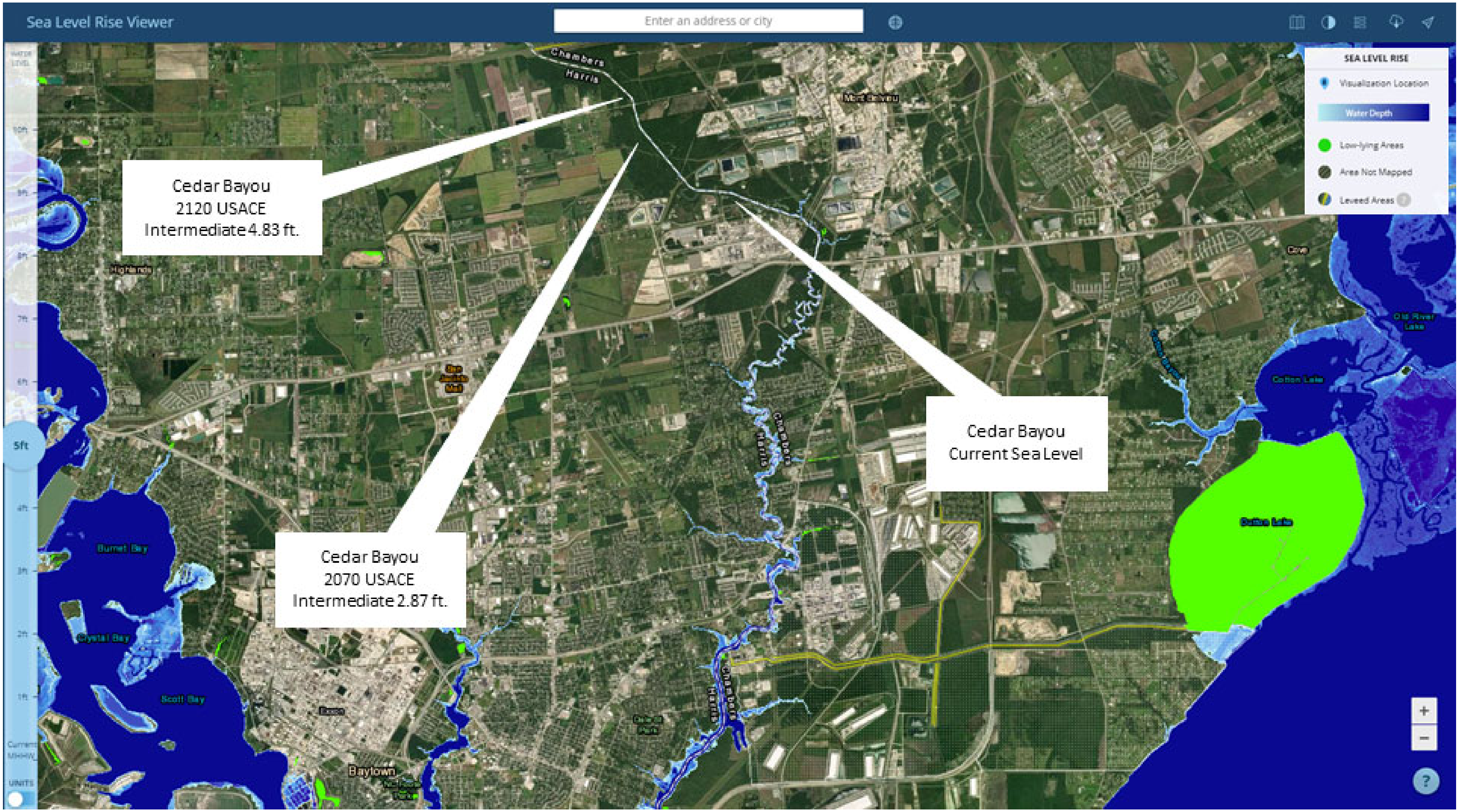

Figure 4 NOAA Sea Level Rise Viewer - Cedar Bayou

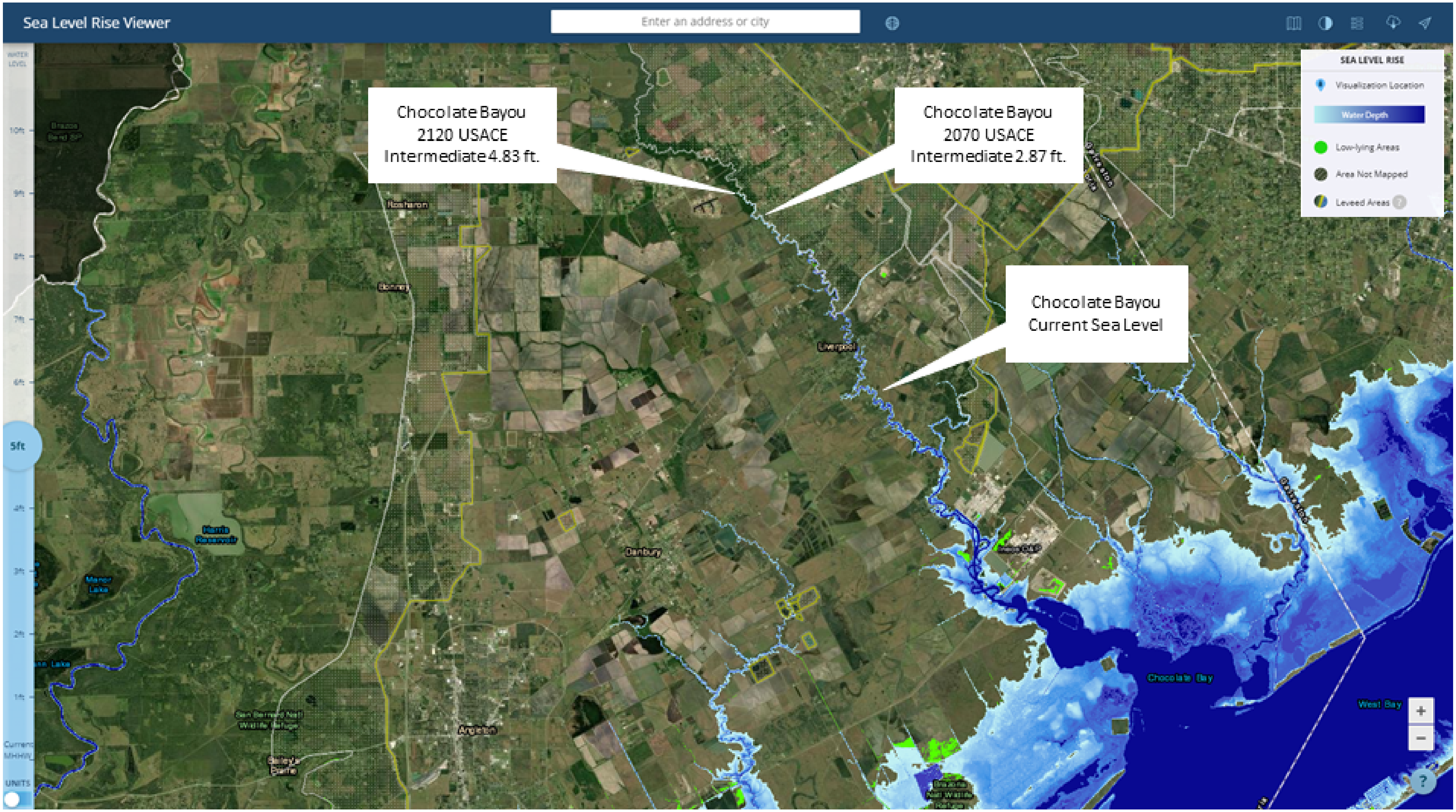

Figure 5 NOAA Sea Level Rise Viewer - Chocolate Bayou

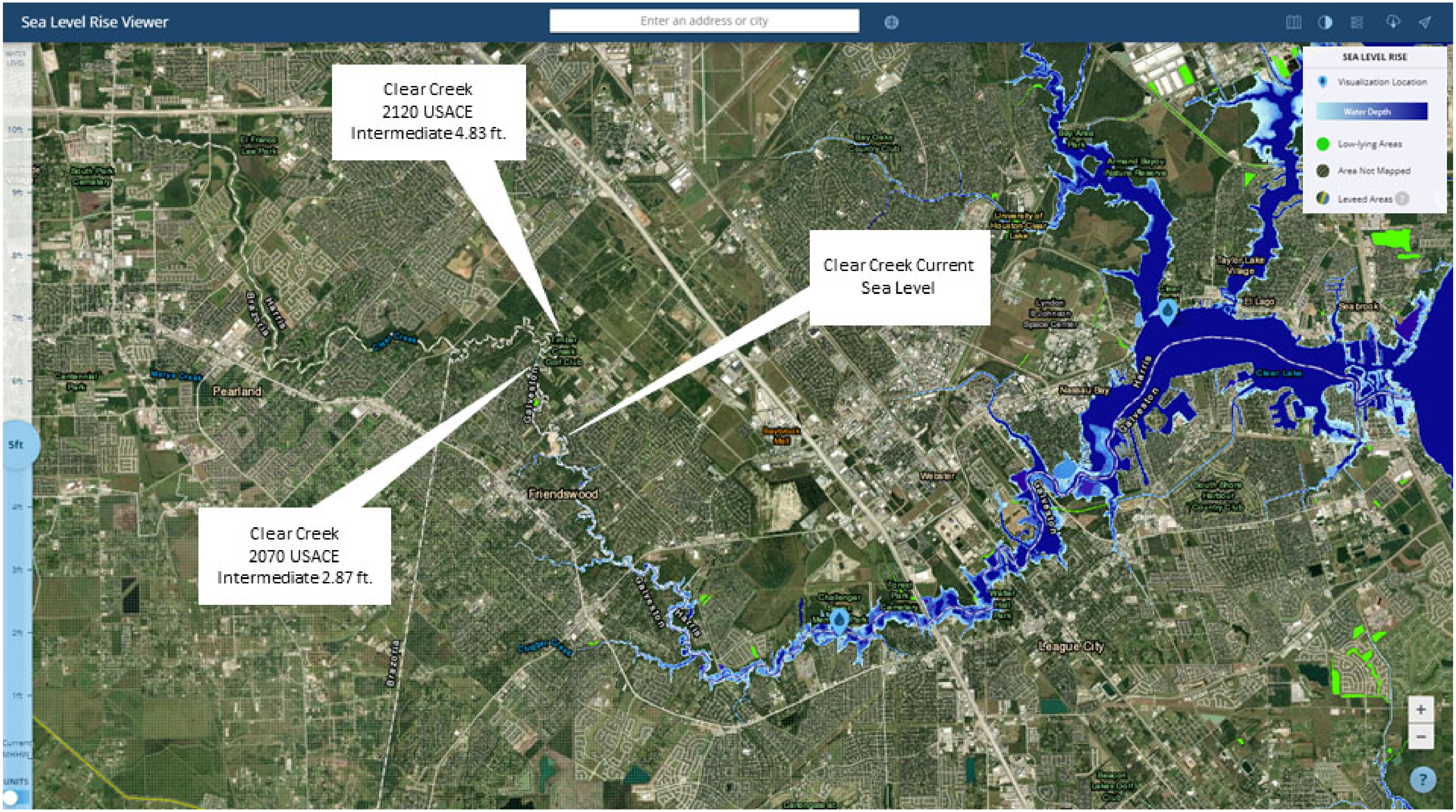

Figure 6 NOAA Sea Level Rise Viewer - Clear Creek

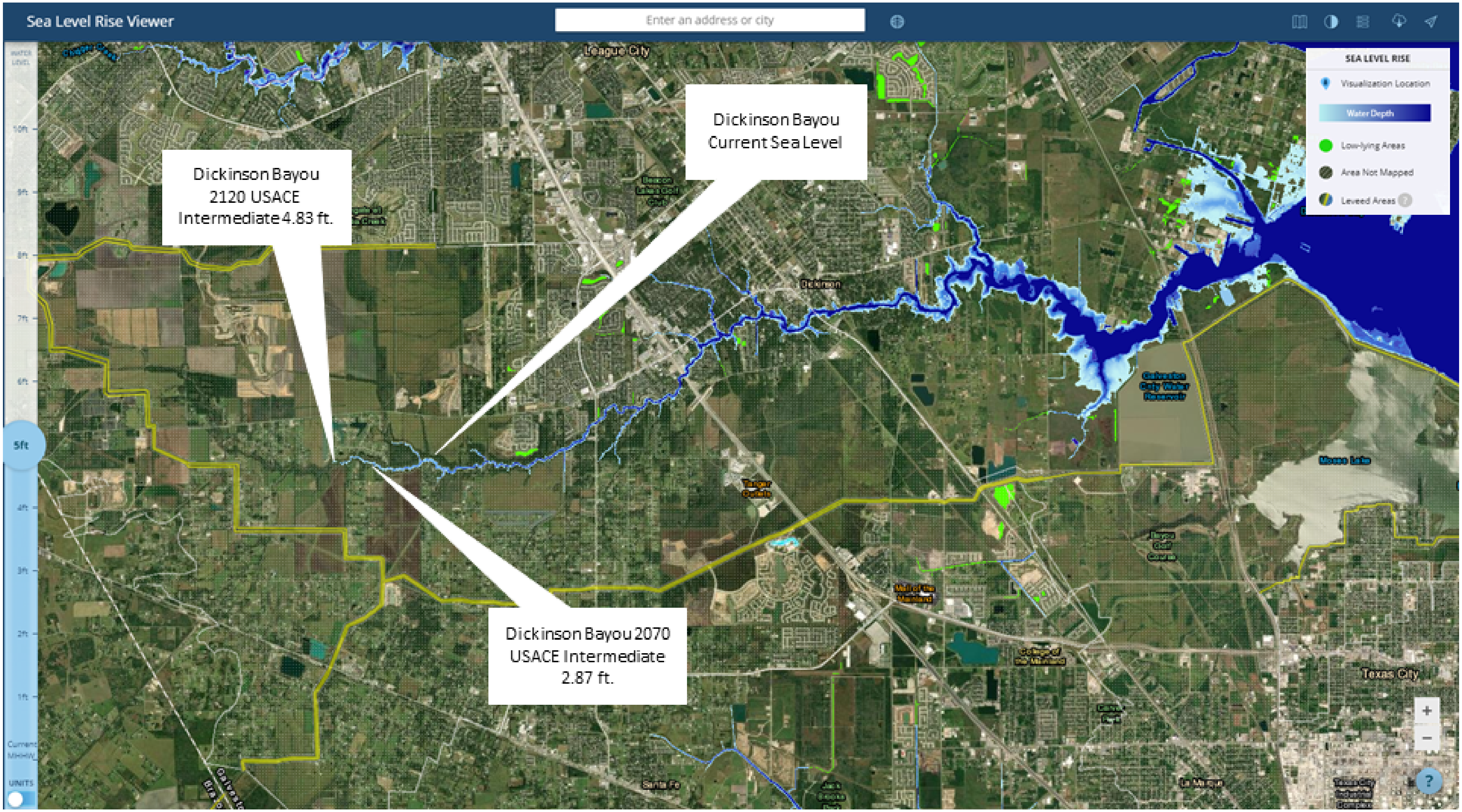

Figure 7 NOAA Sea Level Rise Viewer - Dickinson Bayou

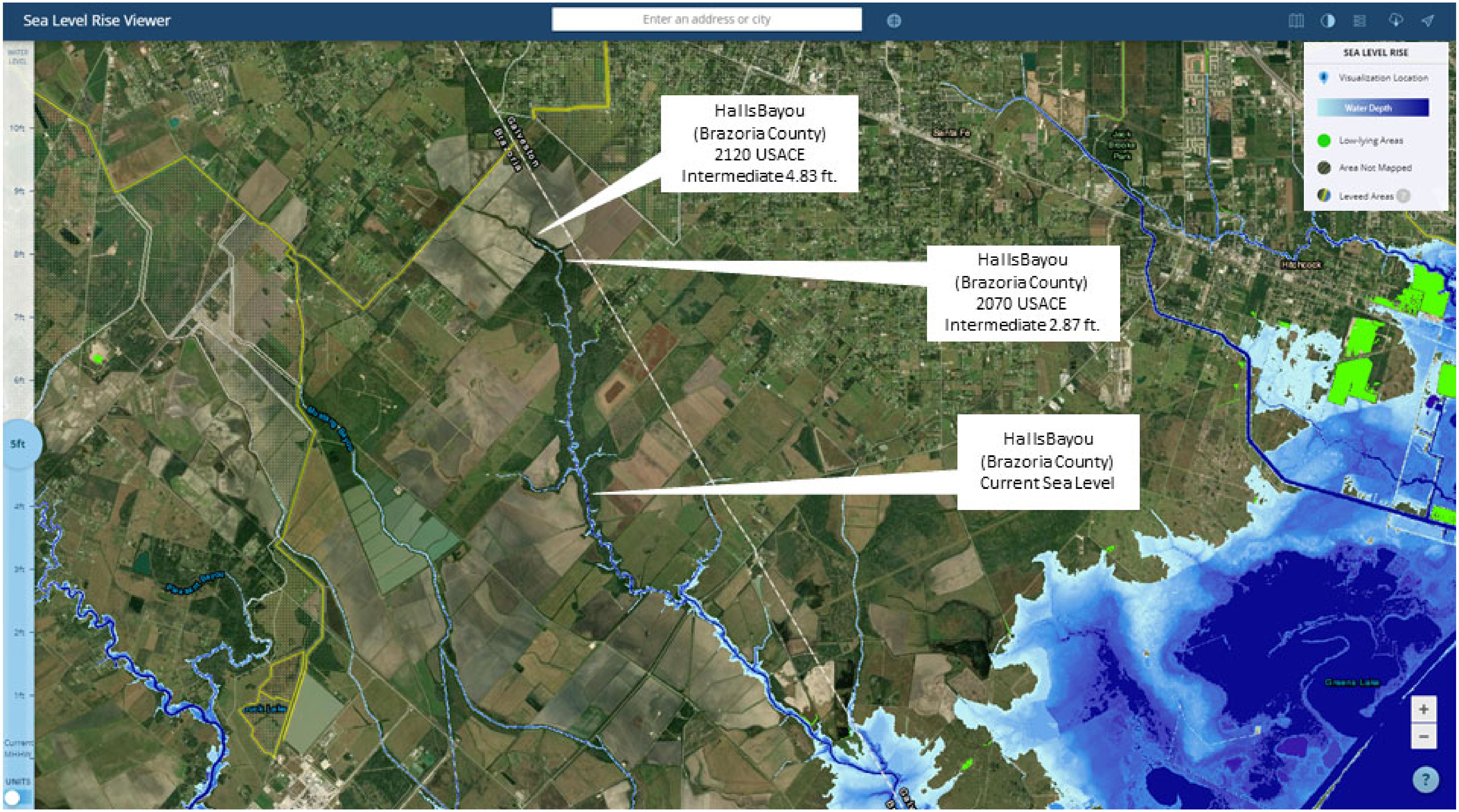

Figure 8 NOAA Sea Level Rise Viewer - Halls Bayou (Brazoria County)

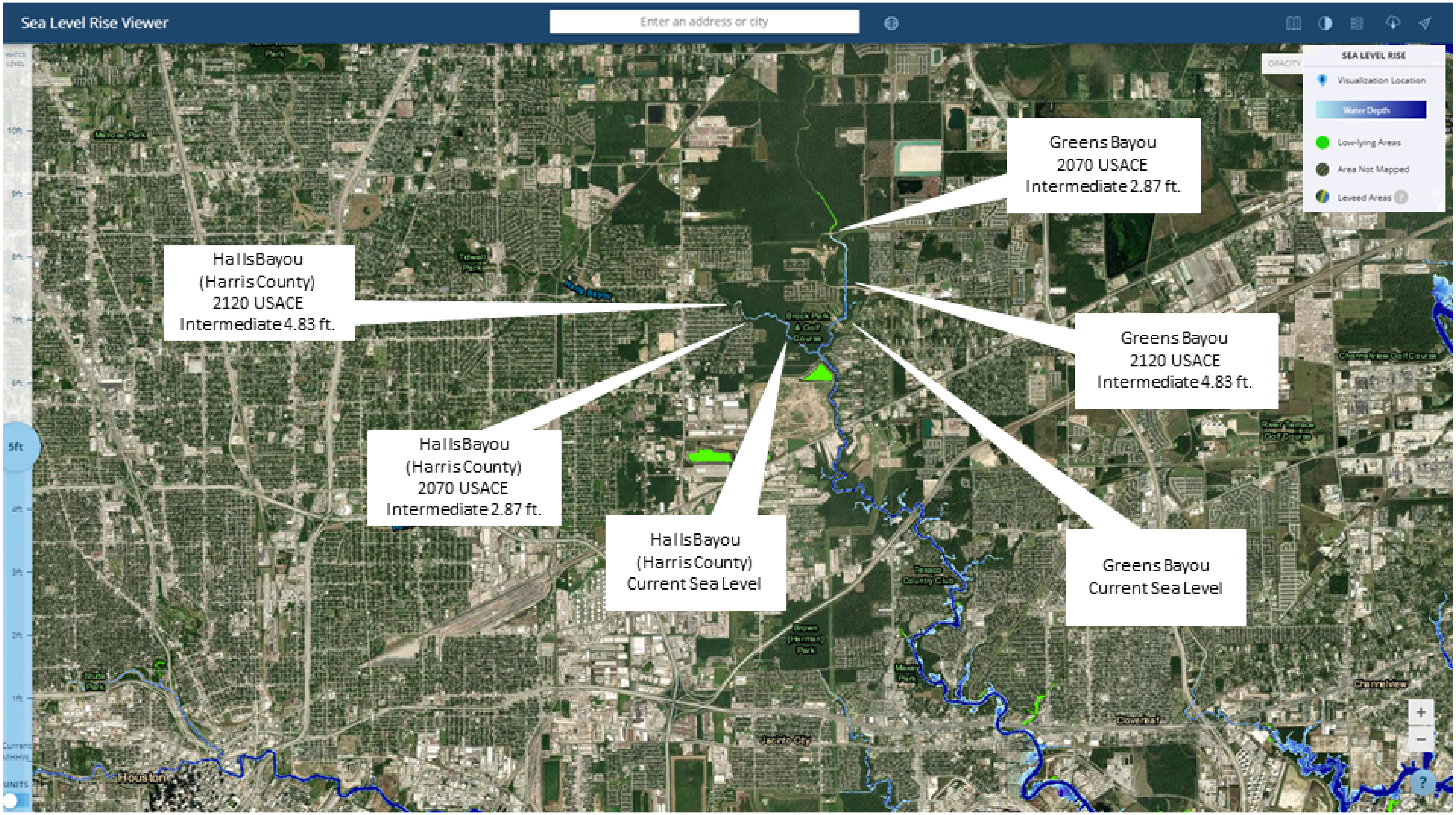

Figure 9 NOAA Sea Level Rise Viewer - Halls Bayou (Harris County) and Greens Bayou

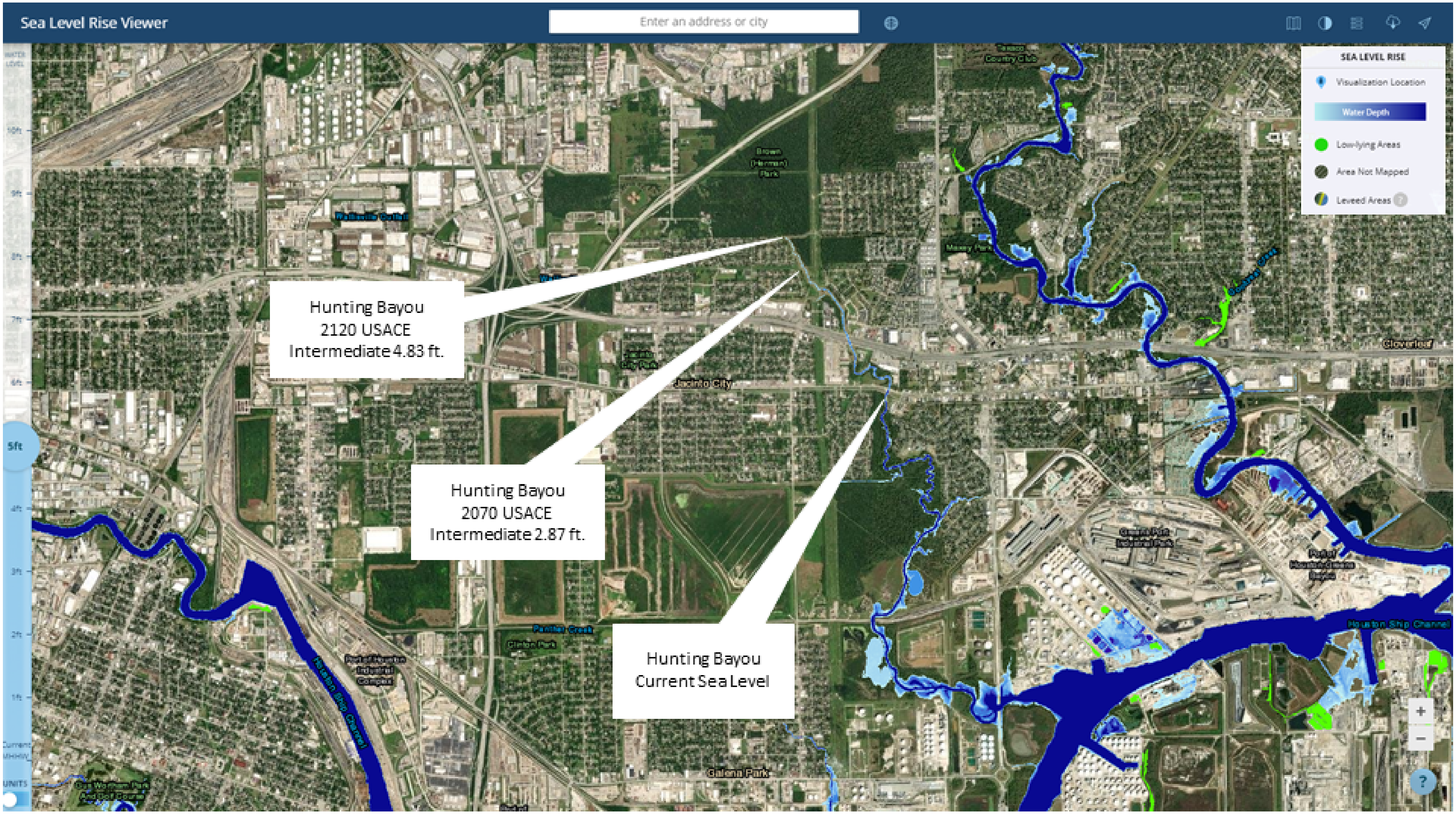

Figure 10 NOAA Sea Level Rise Viewer - Hunting Bayou

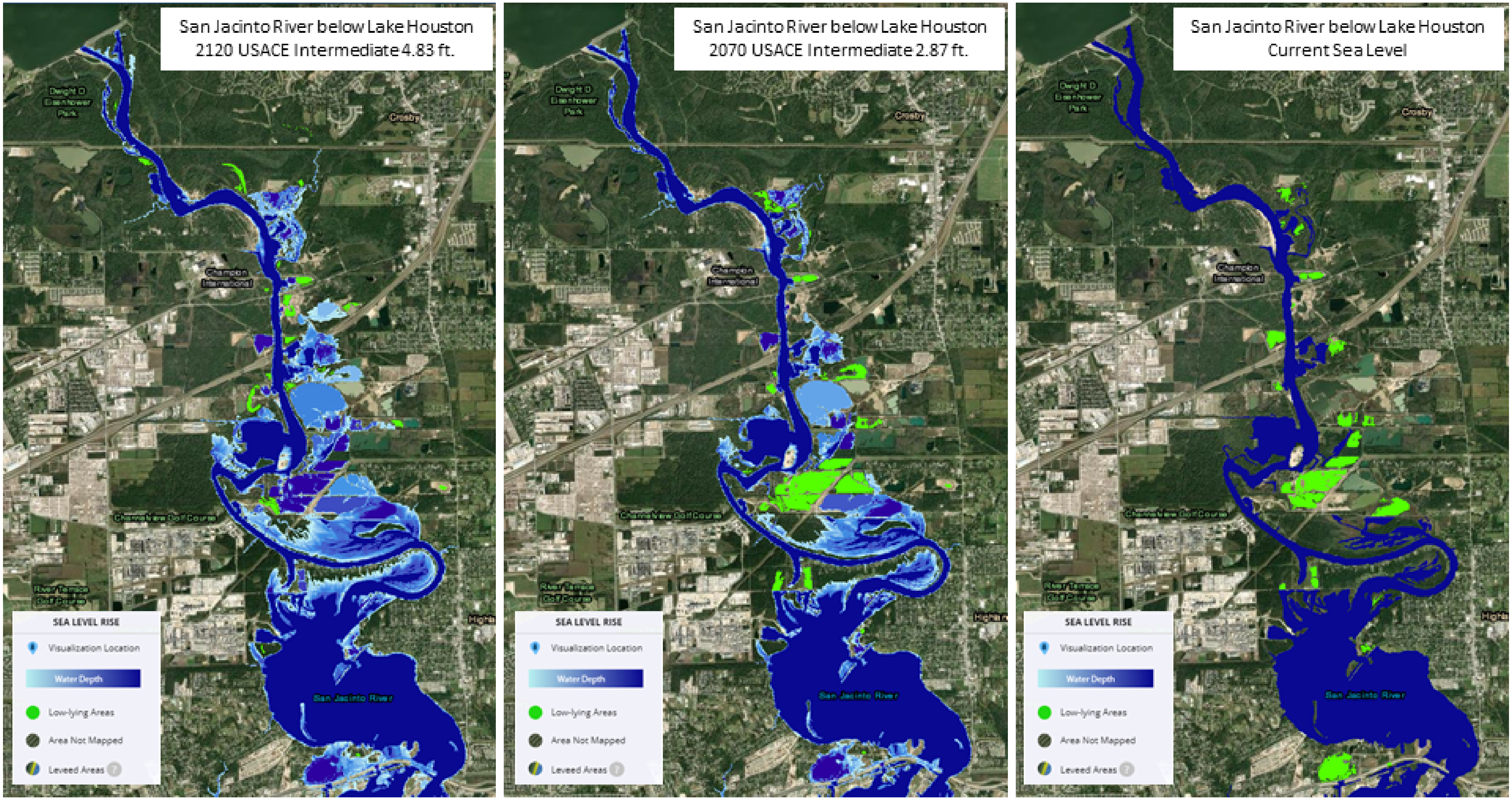

Figure 11 NOAA Sea Level Rise Viewer - San Jacinto River below Houston

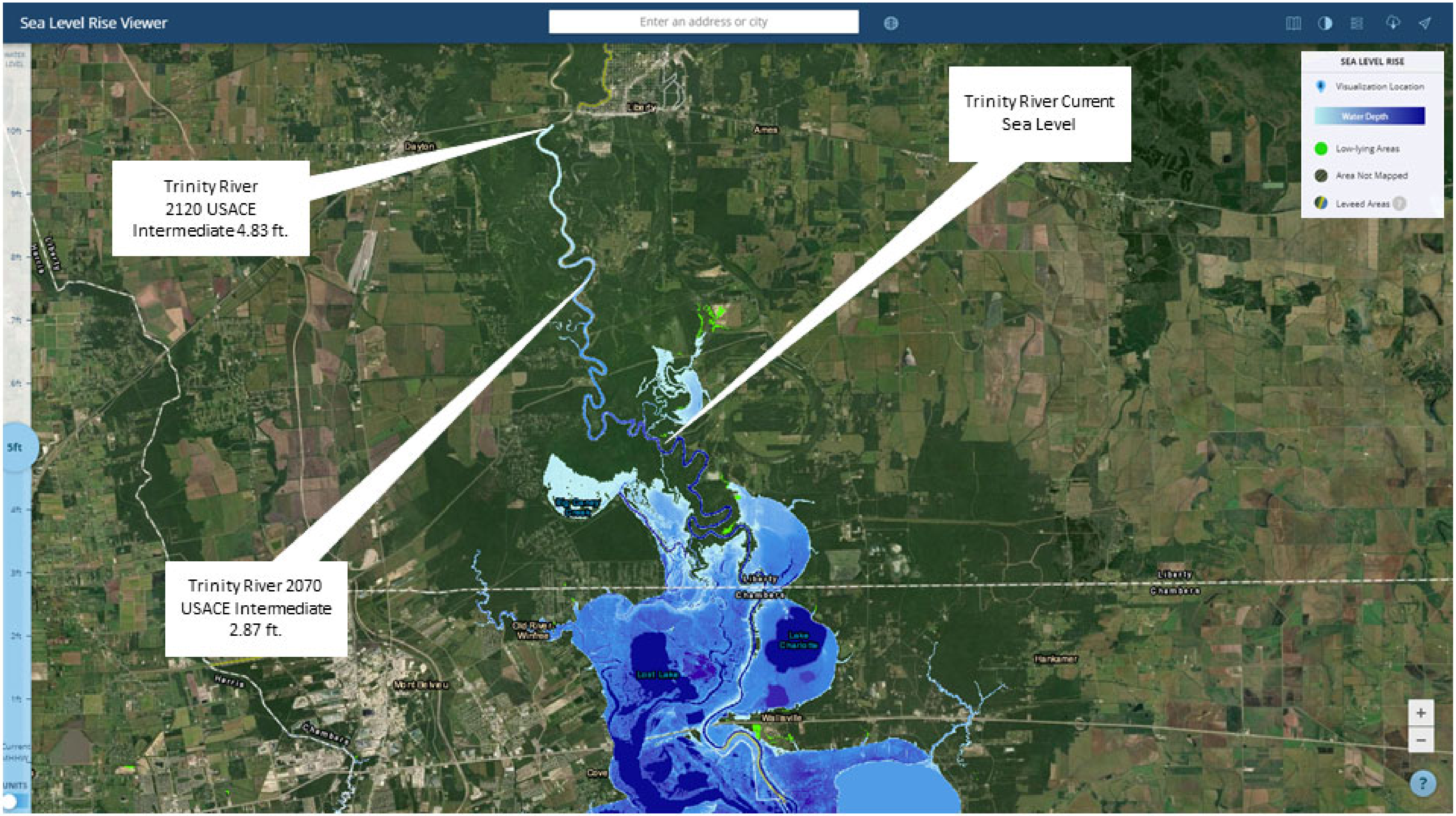

Figure 12 NOAA Sea Level Rise Viewer - Trinity River